Effect of Talc and Vitamin E TPGS on Manufacturability, Stability and Release Properties of Trilaurin-based Formulations for Hot-Melt Coating

Van-Trung-Tin Huynh, Suenia de Paiva Lacerda, Fabienne Espitalier, Eric Beyssac, Maria-Inês Ré

Effect of Talc and Vitamin E TPGS on Manufacturability, Stability and Release Properties of Trilaurin-based Formulations for Hot-Melt Coating

Van-Trung-Tin Huynh[1], Suenia de Paiva Lacerda[1], Fabienne Espitalier[1], Eric Beyssac[2], Maria-Inês Ré[1]

[1]RAPSODEE - Centre de recherche d'Albi en génie des procédés des solides divisés, de l'énergie et de l'environnement, Albi – France

[2]UFR de Pharmacie, Université de Clermont Auvergne, Clermont-Ferrand – France

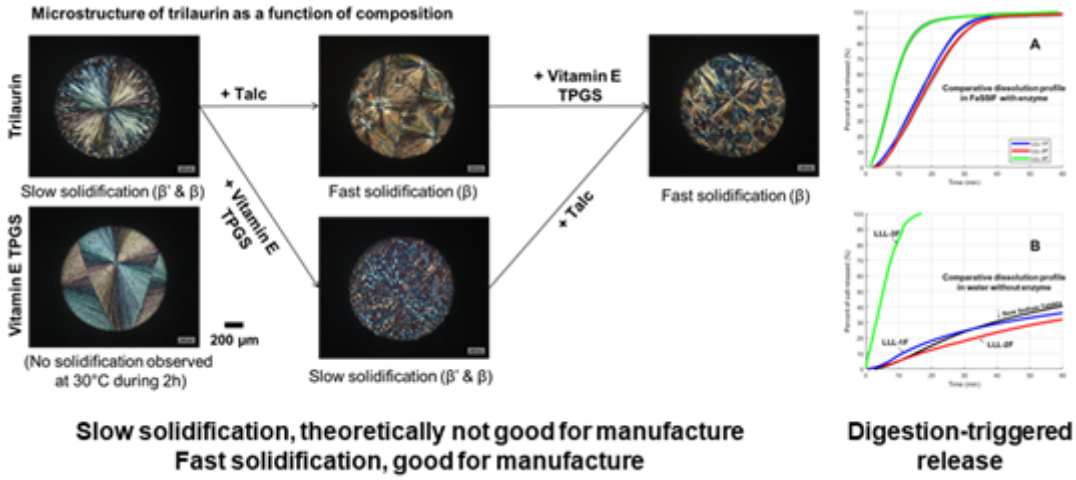

Abstract

This study was focused on one particular case of hot-melt coating with trilaurin – a solid medium-chain monoacid triglyceride. The challenge of using trilaurin as coating agent in melting-based processes is linked to its relatively low melting profile: 15.6°C ($T_{m,\alpha}$), 35.1°C ($T_{m,\beta'}$) and 45.7°C ($T_{m,\beta}$). From a process perspective, the only possibility to generate products coated with formulations composed of trilaurin is by setting thermal operational conditions above $T_{m,\alpha}$. From a material perspective, this processing possibility depends principally on trilaurin crystallisation which was investigated via a set of analytical techniques including turbidimetry, calorimetry, hot-melt goniometry, and polarised light microscopy. A highly soluble drug model substrate (sodium chloride crystals) was coated with three selected trilaurin-based formulations: (i) trilaurin, (ii) trilaurin plus talc, and (iii) trilaurin plus vitamin E TPGS and talc. Coated salt crystals were then analysed to investigate processing performance, coating quality, stability and release properties under digestion effect. The results show that firstly, talc addition promotes nucleation and crystal growth and, as a consequence, it facilitates the manufacture of trilaurin-based formulations. Secondly, the formulation of a solid triglyceride and a hydrophilic surfactant could potentially cause release instability, but formula (iii) was found to be stabilised by a mechanism whereby trilaurin crystallization enhanced in the presence of talc immobilised vitamin E TPGS in its crystal lattice. Thirdly, talc addition did not significantly influence trilaurin digestion which endows products with an immediate release in lipolytic conditions instead of an extended liberation in pure water. Nor did the addition of one or two additives alter the extent of trilaurin digestion under the conditions studied. These important findings relate to product manufacturability, stability, and release properties. A good understanding of material properties (e.g. crystallisation, polymorphism

digestibility) is essential for melt-processing, lipid coating stabilising and modulation of release profile of solid lipid-coated product, as demonstrated in this case study with trilaurin.

1. INTRODUCTION

Hot-melt coating in fluidised bed represents an encapsulation technique whose principles rely on two main processes: (1) transfer of molten material onto surface of substrate particles in fluidisation and (2) formation of a solidified film upon contact with air-cooling (Appelgren & Eskilson, 1993). Without the use of organic solvents or aqueous vehicles, hot-melt coating operations are time-, energy-efficient and environmentally friendly (Becker et al., 2015). They can even become leaner and greener with the approach oriented to direct crystallisation of the most stable polymorph of triglycerides (Lopes et al., 2015). From a process perspective, there has been rarely publications where trilaurin was used for melt-processing. Actually, two studies reported the use of trilaurin with/without polyethylene glycol 10000 (PEG) successfully extruded at 40°C to encapsulate theophylline (Windbergs et al., 2009d, 2009a). It was concluded that the most stable form was achieved at this temperature (Windbergs et al., 2009d). It is noted that even for a mixture of trilaurin-additive-drug 45:5:50 direct crystallisation of β solid form still occurred (Windbergs et al., 2009a). The role of drug and PEG in trilaurin crystallisation represents a question for this application. Otherwise, it was necessary to quench trilaurin melt to 5°C to recover its α solid form with an extreme cooling rate (Takeguchi et al., 2020). These studies highlight the technical challenge of hot-melt coating with trilaurin: temperatures need to be as high as possible to avoid high energy consumption for cooling the inlet fluidization air. This challenge could be solved by using additives, as in the aforementioned studies.

From a material perspective, trilaurin is a monoacid triglyceride the polymorphs of which exhibit low melting points compared to the ambient temperature. If trilaurin solidification is the main factor of processability, both nucleation and crystal growth (two processes of crystallisation) should be considered notably when additives are used. Studies with trilaurin and additives reported in the literature support this hypothesis. Firstly, additive addition was reported to affect crystallisation points of trilaurin using surfactants (Aronhime et al., 1988). Lauric acid and lauric-acid derivatives were concluded to exert contradictory effects (inductor or inhibitor) on trilaurin crystal growth (Smith et al., 1994; Smith & Povey, 1997). Recently, talc, regarded as a new type of additives due to its inorganic nature, was reported to exert an templating effect on crystallisation of triglycerides (Yoshikawa et al., 2014), inducing heterogeneous crystallisation of trilaurin and instantaneous β'-β transformation.

From a products perspective, biopharmaceutical properties of trilaurin appear much overlooked as a matrix excipient. In fact, trilaurin belongs to triglycerides constituted of medium-chain fatty acids (Jadhav & Annapure, 2023) which are normally used to formulate liquid lipid-based bio-enabling formulations (Feeney et al., 2016). These formulations are in favour of pharmacokinetic properties oftentimes owing to their digestibility. Trilaurin is unique with its solid state at room conditions and its susceptibility to digestion in comparison with other monoacid triglycerides made of saturated long-chain fatty acids (e.g., trimyristin, tripalmitin, tristearin) (Christophersen, Vaghela, et al., 2014; Christophersen, Zhang, et al., 2014). On the one hand, fast digestion of trilaurin in alignment with rapid release of a peptide was found to protect it from proteolytic degradation (Christophersen, Zhang, et al., 2014). On the other hand, digestion of trilaurin was reported to be a contributing factor to enhanced bioavailability of drugs (Nishihata et al., 2011; Watanabe et al., 1993; Yoshitomi et al., 2011). In addition, this property has been exploited to design gastro-resistant or enteric coated tablets even with very low concentrations of trilaurin (Yoshitomi et al., 1992, 1993). It should be noted that those dosage forms were prepared with recourse to aqueous vehicles/organic solvents.

To our knowledge, there is no proof of concept of trilaurin-based formulated microparticulate products prepared via melt-processing and no correlation on release of active substance and digestion of lipid coating membrane, as suggested in the literature (Jannin & Cuppok, 2013). The study presented here is to propose trilaurin-based lipid formulations on a particulate substrate for a digestion-triggered release. The effect of two different additives (talc and vitamin E TPGS) to trilaurin was investigated on process manufacturability, stability and release properties of a coated highly soluble model substrate (crystals of NaCl). The choice of this model substrate is due to its high solubility (ideal condition for verifying coating performance) and ease of measurement and kinetic monitoring using conductometric techniques. it is also a representative model of a product of pharmaceutical interest targeting a slow sodium chloride release for the treatment and prevention of sodium chloride deficiency (Clarkson et al., 1971).

Before coating studies, two studies were carried out with trilaurin-based formulations. Firstly, a fundamental study for formulations screening was performed with turbidimetry-integrated Crystal16® for measurements of crystallisation points. A turbidimetry-integrated technique has been used to study lipid crystallisation, as a new application. Then, the trilaurin-based lipid formulations were analysed via calorimetry, goniometry, and polarised light microscopy in order to investigate deeply polymorphism and underlying mechanisms of crystallisation possibly involved in processing. During hot-melt coating study, salt particles coated with trilaurin-based formulations were evaluated to conclude on process performance, coating quality, release properties as well as long-term stability.

2. MATERIALS AND METHODS

2.1. Materials

Trilaurin (LLL, $T_{m,\alpha}$ = 15.6°C, $T_{m,\beta'}$ = 35.1°C, $T_{m,\beta}$ = 45.7°C) and vitamin E TPGS (VitE_TPGS, HLB ≈ 13) were purchased from TCI Europe N.V. and PMC Isochem (France). Luzenac PHARMA M (talc, T) ($d_{50,laser}$ = 10.5 µm) was kindly donated by Azelis (Courbevoie, France). Bile extract porcine (B8631-100G), cholate sodium ($C_{24}H_{39}NaO_5.xH_2O$) (C1254-100G), deoxycholate sodium ($C_{24}H_{39}NaO_4$) (D6750-25G), 4-bromophenyl-boronic acid (B75956-5G), tris-maleate ($NH_2C(CH_2OH)_3.C_4H_4O_4$) (T3128-50G), calcium chloride ($CaCl_2.2H_2O$) (223506-25G) and sodium chloride (NaCl) (S9888-1KG) were purchased from Sigma Aldrich (Merck KGaA, Darmstadt, Germany). Soya lecithin (Lipoid S 100, purity ≥ 94%) was kindly donated by Lipoid (Grasse, France).

Talc was used as an additive who acts a templating agent while vitamin E TPGS should provide a possibility to accelerate release kinetics. Those materials were composed into formulations detailed in **Table 1** and **Table 2.**

Table 1. Lipid-based formulations composition for screening with Crystal16 crystallization systems

Formulation	Excipients (% w/w)		
	LLL	VitE_TPGS	T
LLL	100	-	-
LLL+T 0.1%*	99.9	-	0.1

LLL+T 0.5%*	99.5	-	0.5
LLL+T 1.0%*	99.0	-	1.0
LLL+VitE_TPGS	90	10	-
LLL+VitE_TPGS+T 0.1%*	90	10	0.1
LLL+VitE_TPGS+T 0.5%*	90	10	0.5
LLL+VitE_TPGS+T 1.0%*	90	10	1.0

**** indicates 1.0%, 0.5%, 0.1% w/w talc to the total 99%w/w of other components***

 # denotes that it is only used in preformulation study

Table 2. Lipid-based formulations composition for hot-melt coating

Formulation		Excipients (% w/w)		
		LLL	**VitE-TPGS**	**T**
LLL-1F	LLL	100	-	-
LLL-2F*	LLL+T 1.0%	99	-	1
LLL-3F*	LLL+VitE_TPGS+T 1.0%	90	10	1
LLL-3F-1#	LLL+VitE_TPGS	90	10	-

**** indicates 1% w/w talc to the total 99%w/w of other components***

 # denotes that it is only used in preformulation study

2.2. Methods

2.2.1. Preformulation studies

2.2.1.1. Turbidimetry with Crystal16 Crystallization Systems

One of the objectives of this work was to develop a fast-screening method based on melt crystallisation principles with Crystal16 crystallization systems. To reach this goal, measurements of melting and crystallisation points were performed with Crystal16® 1.5 mL multiple-reactor setup (Technobis Crystallization Systems, Amsterdam, Netherlands). As is stated the principle of turbidimetry, the characterisation consists of measuring disappearance or appearance of melting or crystallising solids in molten media at a specific timepoint or temperature, respectively.

About 700 mg of each formulation listed in **Table 1** was weighed and introduced in a 1.5 mL vial of specific design. This quantity was found sufficient to cover the light transmission pathway. After preliminary trials, bottom stirring mode was chosen and a stirring rate was set at 200 rpm, which assures homogeneous mixing of molten media. A typical run programme is illustrated in **Figure 1**. Firstly, it starts when heating is launched till 100°C and held for 10 min at this point to completely melt all the crystals. Then the first step of "tuning" will be performed to reset the transmissibility through one block (4 vials) to 100% as there might be a difference due to mixing heterogeneity. Cooling is performed at 20°C/min from 80°C till 46°C – $T_{m,\beta}$ of trilaurin. At this point, the second step of "tuning" is performed so as to reset all the transmissibility values to zero as they might diminish with temperature decrease. From 46°C to 20°C a cooling rate of 0.05°C/min is defined as the condition for non-isothermal crystallisation. When the programme temperature reaches 20°C (temperature at which all the trilaurin-based systems should be solidified), the system will be heated again up to 50°C at the same velocity. The objective of this last step is to measure melting point of the system. Onset melting point or crystallisation point are identified as the temperature at which the transmissivity starts to increase or decrease significantly, accordingly.

As shown in **Figure 1**, by definition, the difference of melting point and crystallisation point is the width of metastable zone (Kulkarni et al., 2013), which will be considered as proof of thermal feasibility of tristearin under the effect of different additive-combinations. In addition, non-isothermal experiments were also conducted with a cooling rate of 5°C/min and 10°C/min, which might represent the cooling capacity of certain melt-processing technologies. The measurements for each formulation were performed in triplicate (n = 3).

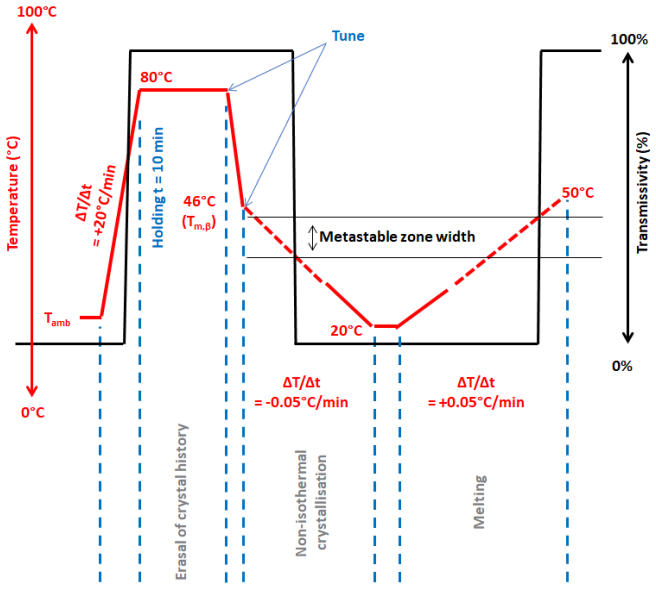

Figure 1. Thermal programme set for non-isothermal experiments in Crystal16®

2.2.1.2. Differential Scanning Calorimetry (DSC)

Thermal properties of formulations such as melting point (T_m), phase transitions are studied using DSC Q200 (TA Instrument, USA). All the analyses are performed in non-hermetic aluminium pans under nitrogen purge at 50 mL.min^{-1}. For isothermal crystallisation, the thermal programme, spanning over a temperature range of 0°C and 100°C, consists of holding time for 2h at 30°C followed by a second heating, for which a heating rate of 30°C min^{-1} is chosen as this rate allows for net separation of thermal events (Takeguchi et al., 2020) and as a result polymorphic identification. Thermal data in the isothermal crystallisation step is further exploited to construct solidification profile, i.e. solid fraction content (SFC) (%) as a function of time with the following formula (Müller et al., 2018; Rigolle et al., 2018):

Equation 1 :

$$SFC(t) = \frac{\int_0^t h dt}{\int_0^{t_\infty} h dt} \times 100 = \frac{\int_0^t h dt}{\Delta H_c} \times 100$$

where h is specific heat flow at the time t (W/g) and ΔH_c is the crystallisation enthalpy of the formulation (J/g).

2.2.1.3. Measurements of Contact Angle

To evaluate the wetting behaviours of coating formulations and therefrom induce their affinity to the substrate, measurements of contact angle in molten state were performed with the experimental setup shown in **Figure 2,** developed for this purpose. It comprises (1) a metallic insulated envelope accommodating (2) the dosing syringe capable of controlling heat by water current and (3) a chamber equipped with a Platin plate whose temperature is controlled by electricity. This chamber is placed on (4) a support (DSA30, Kruess) the height of which can be adjusted manually, and its internal temperature is verified using an external numerical thermometer (Chauvin Arnoux C.A 861). For image acquisition, (5) a camera lens (Namitar 1-6010) fixed at x 0.7 magnification and (6) a tungsten light (dedolight DLH4) of 3400K intensity is placed in opposite positions. (7) Image acquisition and analysis is piloted by the software DSA4. Each formulation was melted beforehand in an oven at 80°C, agitated and poured into a single-use 1 mL syringe. The latter is then placed in the heat-control box of the goniometer. For each formulation, measurements (n = 3) were performed at a temperature close to that of fluidisation temperature – 30°C – at a distance of 5 cm as this allows for good observations of film formation in the course of liquid-solid transitions. During a measurement, the evolution of droplet was captured each in a 10-minute video at a rate of 1 frame per second. Solidification time was directly estimated from taken images. The substrate was salt pastilles produced using a hydraulic press Atlas Power T15 Specac 13 mm die. About 1.7 g of fine salt was compressed under a pressure of 2 tons during 15 s as relaxation time and the surface of pastilles generated in this manner was sufficiently smooth.

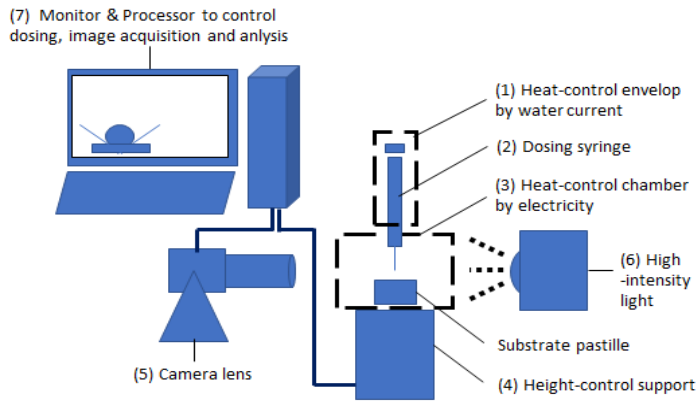

Figure 2. Simplified experimental setup for measurements of contact angle in molten state

2.2.1.4. Polarised Light Microscopy

Polarised images were acquired using Zeiss IMAGER.M2m powered by Power Supply 232, equipped with a tube lens 1.25x and external long-distance objectives 5x and 20x for use with a heating plate. In addition, automatic image acquisition was conducted by the camera Aixocam 305 Color and 10x magnification should aslo be considered. A polarised angle of 75° was chosen for all observations. Light intensity was manually set at about 80% on the date of observation. Four formulations were prepared on lamellas using thermal conditions mimicking coating operations: holding at 80°C for 5 min and cooling at 10°C/min till 30°C and holding at this temperature till complete crystallisation. These lamellas were then used for the whole stability study. Four to six images were taken for each time of observation, i.e. freshly after preparation t_0, 6 weeks and 12 weeks after.

2.2.2. Hot-Melt Coated Products: Preparation and Characterisation

2.2.1. Hot-Melt Coating (HMC) Processing

HMC trials were performed using lab-scale Ventilus® airflow technology (Romaco© Group, Germany) which is demonstrated in **Figure 3**. Process parameters are presented in **Table 3**. Before each coating trial, the process chamber was pre-heated with the entry of fluidisation and atomisation air flows. The substrate particles were then introduced to equilibrate with the temperature briefly and the coating operation was initiated. In the course of one trial, regular sampling was carried out at the moment where one target coating content was targeted, i.e. 10%, 20%, and 30% w/w and the feeding rate was calculated based on the mass of coating agent delivered in the intervals of one or two minutes. In this study, coating content is defined as the mass percentage of coating material present in the finished product. After each coating operation, the yield (%) is calculated based on the mass balance:

Equation 2 :

$$Yield\ (\%) = \frac{m_{tot,\,sampled} + m_{tot,recovered}}{m_{substrate} + m_{ca,dispensed}} \times 100\%$$

where, $m_{tot,\,sampled}$ is the total mass of samples taken during the coating trial (g), $m_{tot,recovered}$ the total mass of coated product obtained at the end of trial (g), $m_{substrate}$ and $m_{ca,dispensed}$ the total mass of substrate and that of coating agent dispensed for the trial (g), respectively.

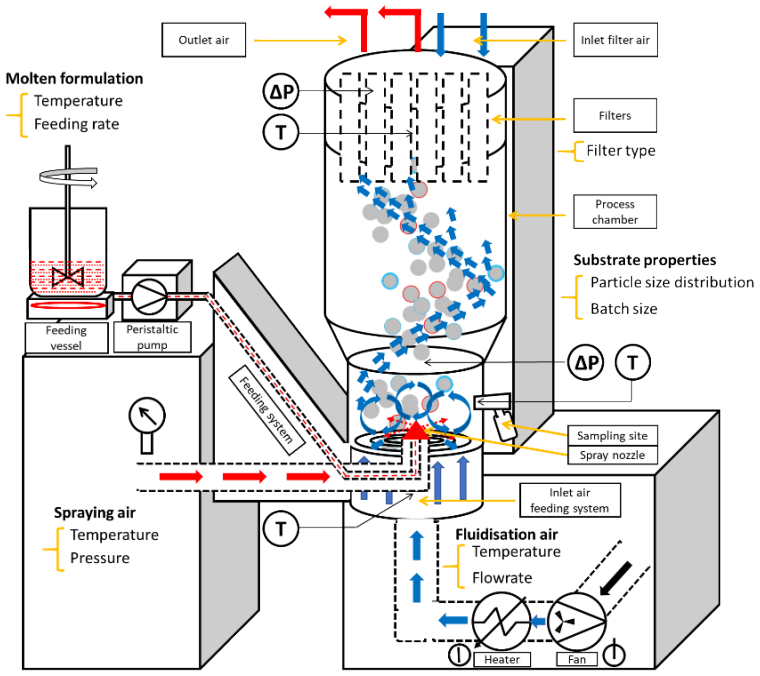

Figure 3. Schematics of Ventilus® airflow bed in coating operation

Table 3. Process parameters and their values specified for hot melt coating of LLL-1F, LLL-2F and LLL-3F

Parameters	Set-up values
Reactor volume (L)	1
Batch size (g)	250
Final coating content (% w/w)	30
Temperature of fluidisation air (°C)	30 (setpoint)
Quantity of process air (m^3/h)	37
Temperature of melt media (°C)	80
Temperature of feeding system (°C)	80
Temperature of spraying air (°C)	80
Pressure of spraying air (bar)	0.5

Formulation feeding rate (g/min):	≈ 18-19 (LLL-1F, LLL-2F) ; ≈ 24-25 (LLL-3F)

2.2.2. Product Characterisation

Assay of Coating Contents

To evaluate process efficiency, assay of lipid content was performed. Lipid-based coating content was indirectly assayed by quantification of salt amount by conductometry (CDM10 model, RadiometerLab, Copenhagen). In a glass flacon 80 mL, around 40 mg coated products were firstly wetted with about 5 mL of ultrapure water and then heated at 100°C to melt lipid envelope. Next, about 55 mL of ultrapure water was added to dissolve salt contents and conductivity measures were performed. Assay was carried out in triplicate (n = 3) via gravimetrical method. Before analysis conductivity sensors were calibrated with a conductivity standard solution 1413 µS/cm at 25°C (Hamilton, USA). After that, the efficiency of coating process is evaluated based on the following formula:

Equation 3 :

$$Efficiency = \frac{m_{ca,assayed}}{m_{ca,dispensed}} \times 100$$

where $m_{ca,assayed}$ is the real amount of coating agent assayed in the final product and $m_{ca,dispensed}$ the total amount of coating agent dispensed at the moment of sampling. $m_{ca,assayed}$ and $m_{ca,dispensed}$ are used to calculate the practical and theoretical coating content, i.e. the mass percentage of coating formulation recovered in the finished product.

Particle Size Distribution

Measurements of particle size distribution (PSD) were performed using laser diffraction particle size distribution analyser Mastersizer 3000 (Malvern Instruments, Malvern, United Kingdom) under dry dispersion mode. The mean size of the population of particles is expressed *in* $D_{[4,3]}$. Both PSD in number and volume were considered to identify the process regime. Two PSD parameters, i.e. PSD width (SPAN) and the ratio $\mathrm{D_{v(90)}}/\mathrm{D_{v(90)}}$, are calculated from or $\mathrm{D_{v(10)}}$, $\mathrm{D_{v(50)}}$ and $\mathrm{D_{v(90)}}$ from the expression given below:

Equation 4 :

$$SPAN = \frac{D_{v(90)} - D_{v(10)}}{D_{v(50)}}$$

where, $\mathrm{D_{v(10)}}$, $\mathrm{D_{v(50)}}$ and $\mathrm{D_{v(90)}}$ represent the maximal particle size of 10%, 50% and 90% volume of the whole particulate population.

X-ray powder diffraction

Polymorphic identification with X-ray powder diffraction was conducted using Malvern PANalytical Empyrean with reflection applied. The device is equipped with an anticathode tube (radiation Cu Kα ($lamda =$ 1.5418 Å)) and a 1Der X-ray detector. Diffractograms were collected using X-ray source at 45 keV and 40 mA over a 2θ range from 1° to 30° recorded at every step of 0.033° (2) with an acquisition time of 135.255 (or 280.035) s per step. The powder was filled in a sample holder and rotated at 2 s/revolution. Short d-spacing was calculated using the following expression (Schertel et al., 2021):

Equation 5 :

$$d - spacing = \frac{order\ of\ reflection\ (n) \times wavelength\ (\lambda)}{2 \times sin\theta}$$

Crystallite size of tristearin β was estimated approximately from the peak (003) in X-ray powder diffraction patterns, after being fitted with the function Pearson VII, using Scherrer's equation (Lopes et al., 2015):

Equation 6 :

$$D(003) = \frac{K \times \lambda}{FWHM \times \cos\theta}$$

where FWHM is the width in radians of the diffraction maximum measured at half-way height between background and peak, typically known as full width at half maximum (FWHM), θ is the diffraction angle, λ is the X-ray wavelength (1.5418 Å). K (Scherrer constant) is a dimensionless number that provides information about the shape of the crystal and in case of the absence of detailed shape information, $K =$ 0.9 is a good approximation for spherical geometry.

Dynamic Vapour Sorption

Dynamic vapour sorption profiles were recorded using a DVS Resolution instrument (Surface Measurement Systems, London, UK). Samples were loaded onto the quartz balance and dried at 25°C and 0% RH (setpoints) until a constant weight was reached. Next, the relative humidity was increased from 10% up to 95% with a step size of 5-10% with the condition that a minimum equilibration time of 5 minutes was achieved when change in mass remained less than 0.01%. Otherwise, the relative humidity continued to increase/decrease when the holding time at that step attained 360 minutes. The temperature was maintained 25°C (setpoint) during the measurements.

Stability Monitoring

Coated products with three formulations were stored **open** in a climatic chamber (Memmert, Germany) under tempering conditions of 25°C/60%RH. Characterisation techniques involved in stability study consist of XRPD, DSC, DVS, PLM and release testing. All products were analysed at three time points: t_0 (freshly produced), t_1 (6 weeks after), t_2 (12 weeks after).

Release Kinetics

Release in water

Release kinetics of coated salt was obtained with a USP type II apparatus (paddle) (ERWEKA DT light, Heusentamm, Germany). A quantity of coated products equivalent to 600 mg NaCl was placed inside a 100-mesh sinker basket with lid (316 SS). A quantity of glass beads (160-200 µm) equivalent to one quarter of substrate total mass was introduced to prevent agglomeration inside the sinker, strategy already in use in the literature (Frenning et al., 2003). Each test was performed in 250 mL ultrapure water at 37 ± 1°C, under 100 rpm stirring. Conductivity values were automatically recorded every 5s using three conductivity meters (two models CDM10, RadiometerLab, and one model pHenomenal® CO 3100 H, VWR). Before analysis, conductivity sensors were calibrated with a conductivity standard solution 1413 µS/cm at 25°C (Hamilton, USA). For each sample, release testing was performed in triplicate (n = 3).

Digestibility in fasted state simulated intestinal fluid.

Digestibility of selected trilaurin-based coating formulations was investigated with a pH STAT Titrando 901 (Metrohm, Switzerland) equipped with a dosing unit Dosino 800 (Metrohm, Switzerland) and a thermostat (LUDA, Germany). For each experiment, a 100-mesh stainless steel sinker basket containing an amount of coated salts equivalent to 500 mg trilaurin was placed into 36 mL of fasted-state simulated intestinal fluid (FaSSIF) at 37°C with continuously stirring. The detailed composition of FaSSIF used is given in **Table 4**. Pancreatin extract was prepared by dispersing 1.28 g of porcine pancreatin powder (containing pancreatic lipase and co-lipase) to 5.2 mL tris-maleate buffer pH 6.5, following standard dissolution preparation conditions (Arnold et al., 2012). Activity of lipases in pancreatin was priorly assayed following a standardised method (Brodkorb et al., 2019). After dilution with FaSSIF, the final medium should have an activity of about 286 TBU/mL state, i.e. about a half of the reported fasted state activity (Christophersen, Vaghela, et al., 2014). Pancreatin extracts were prepared at the start of a week and stored in freezer for a series of experiments. Before use, the frozen pancreatin extract was thawed at room temperature. The whole digestion medium was titrated to the setpoint pH 6.5 immediately after addition of the thawed pancreatin extract into the reactor. The pH was kept around 6.50 ± 0.05 by titrating with 0.2 M NaOH in the pH-Stat automatic titration unit. The digestion experiments were only initiated at the time of adding the substrate. At the end of 3-hour digestion, a volume of 200 µL 4-bromophenylboronic acid 1 M in methanol was added to stop lipolysis. Then, back titration was performed till pH 9.0 would be reached using the same titrant. For each sample, release testing was performed in triplicate (n = 3). Extent of digestion (%) was estimated using the following equation:

Equation 7 :

$$Extent\ of\ digestion\ (\%) = \frac{n_{FA,\ ionised} + n_{FA,non-ionised}}{n_{max,\ FA\ in\ LbF}} \times 100$$

where $n_{FA,\ ionised}$ number of moles ionised, fatty acid neutralised by NaOH 0.2 M at pH 6.5 (mol), $n_{FA,non-ionised}$ number of moles non-ionised fatty acid back-titrated at pH 9.0 (mol), $n_{max,\ FA\ in\ LbF}$ number of moles fatty acid occurring in the lipid-based formulation (mol).

Table 4. FaSSIF composition

Component	**Concentration**
Bile micelle containing preparation	
Bile extract porcine	Equivalent to 3.0 mM taurocholate sodium
Cholate sodium ($C_{24}H_{39}NaO_5.xH_2O$)	
Deoxycholate sodium ($C_{24}H_{39}NaO_4$)	
Soya lecithin	0.75 mM
Tris-maleate buffer pH 6.5	

Tris-maleate ($NH_2C(CH_2OH)_3.C_4H_4O_4$)	2.0 mM
Calcium chloride ($CaCl_2.2H_2O$)	1.4 mM
Sodium chloride (NaCl)	150 mM

Release studies from coated salt under digestion.

The same apparatus and procedure used for digestibility studies of selected trilaurin-based coating formulations were applied here, with the following adjustments. For each experiment, amounts of coated salts equivalent to 120 mg NaCl (downscaled) were used. The composition of FaSSIF was slightly modified to exclude any presence of NaCl to enable conductivity measurement within the range of validity of the calibration standard. Salt release kinetics was monitored directly and continuously using the conductivity meter pHenomenal® CO 3100 H (VWR). For each sample, release testing was performed in triplicate (n = 3).

Statistical data analysis.

Statistics-based method (Yuksel, 2000) at specific time points 5, 10, 15, 30, 45 and 60 minutes of release testing. This method was chosen to assure statistical meaning due to a limited sample number.

3. RESULTS AND DISCUSSION

2.3. Solidification properties of trilaurin-based coating formulations

2.3.1. Non-Isothermal Crystallisation

The aim of this study was to measure melting and crystallisation points of trilaurin (LLL). Four levels of talc concentration, 0, 0.1%, 0.5% and 1.0% w/w, were investigated to test impact of talc and its concentration on thermal behaviours of this triglyceride and then to select a good level for use in hot-melt coating formulations. Talc concentration was limited to the maximal value of 1.0% w/w in order to avoid segregation in molten state (Beaupere et al., 2018).

Figure 4 shows MZSW map constituted by melting and crystallisation points measured for all the trilaurin-based formulations, showing the width of the metastable zone (MSZW). In melt crystallisation, MSZW could be construed as the difference between the melting point of a solid form and its corresponding crystallisation point measured at a certain cooling rate. In other words, one MSZW applies to each polymorph of a triglyceride but one MSZW map could serve as a guide for melt-processing of that triglyceride.

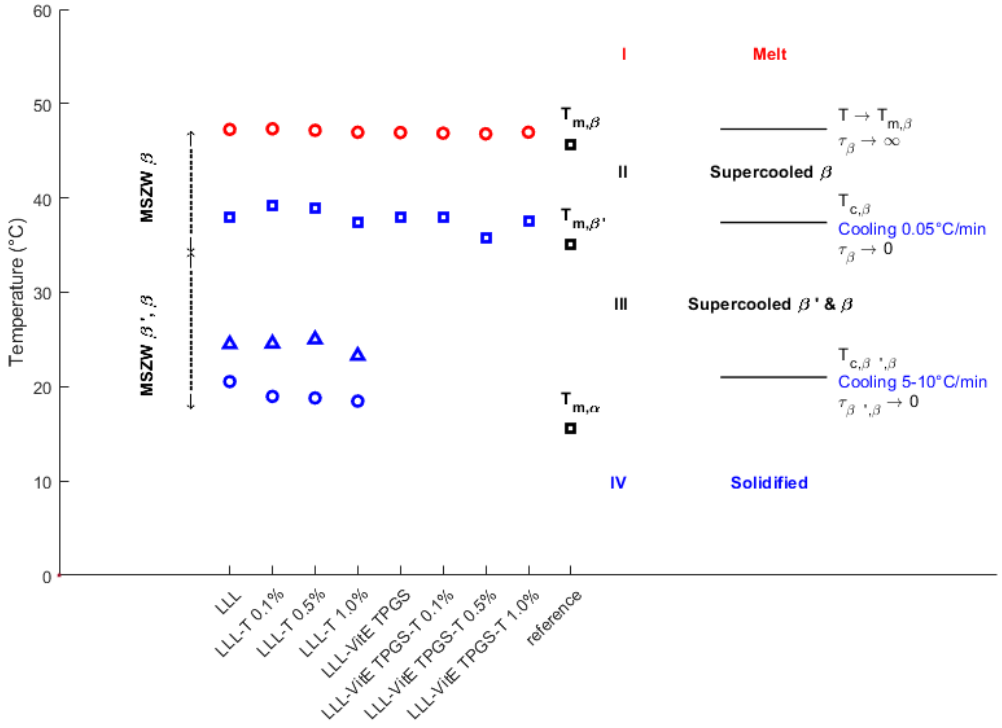

Figure 4. MSZW map measured for all formulations containing trilaurin, with 4 levels of talc concentration (with and without vitamin E TPGS as second additive). Melting points at 0.05°C/min (red circles), crystallisation points at 0.05°C/min (blue squares), 5°C/min (blue triangles) and 10°C/min (blue circles), reference melting points of polymorphs α, β' and β (black squares)

As indicated by the column to the right of measured melting and crystallisation points, MSZW map of LLL based formulations could be divided into 4 regions: I, II, III, and IV. In effect, above the liquidus line of β (I) indicated by the experimental melting temperature of pure β LLL ($T_{m,\beta}$ = 47.3 ± 0.1°C), LLL remains in molten state. At $T_{m,\beta}$, its induction time of β approaches the infinity. In this case study, MSZW (II) where the triglyceride in general and β LLL in particular is supercooled was identified by melting and crystallisation points ($T_{c,\beta}$ = 38.0 ± 1.9°C) measured at 0.05°C/min heating and cooling, respectively. The values of measured $T_{m,\beta}$ of LLL based formulations are close to the reference value (Moorthy, 2018) as this discrepancy could be explained by the fact that $T_{m,\beta}$ varies as function of crystallite size in the sample (Takeguchi et al., 2020). Down from $T_{c,\beta}$ to $T_{c,\beta',\beta}$ lies the region where both β' and β LLL (III) are supercooled and they can nucleate at any time. For LLL, the length of constituent fatty acid chains is shorter, therefore β' LLL is more stable and can occur upon cooling (Yoshikawa, 2016). Below $T_{c,\beta',\beta}$ measured at 5°C/min and 10°C/min (IV), LLL solidifies spontaneously. As a possible application, MSZW map could serve as a guide to choose a thermal condition corresponding to formation of a specific polymorph. Except the region (I) where LLL occurs in molten state, all the 3 remaining regions could be considered for crystallisation of an LLL polymorph in final products. For instance, in a study reported in the literature, successful extrusion of a binary mixture of drug and β SSS LLL conditioned by setting a processing temperature of 40°C which falls within the β MSZW (II) (Windbergs et al., 2009d). In another study, it was reported than even when adding 10% w/w polyethylene glycol (PEG) to the binary system, β LLL could be also obtained at 40°C (Windbergs et al., 2009a). In these cases, drug and PEG can either have no effect on LLL crystallization or be a nucleation inductor.

Definition of thermal conditions in the region (III) where β' and β are likely in the state of undercooling, respectively, was possible in preliminary trials with hot-melt coating when the temperature of fluidisation air (inlet air) was kept at 20-25°C. Several fundamental studies reported a multiplicity of

cases where β' LLL was generated (Kellens et al., 1991; Takeguchi et al., 2020; Windbergs et al., 2009b). β' LLL is more stable than α LLL but the former is converted overnight into β LLL at room conditions (Windbergs et al., 2009b). Direct crystallisation of β LLL was possible at the same thermal conditions with the addition of an additive (Yoshikawa, 2016; Yoshikawa et al., 2014, 2015). In the last region (IV) of LLL MSZW map, in order to obtain α LLL it is necessary to quench the melt at an extreme cooling rate (Takeguchi et al., 2020). It implies that this approach is not technically viable for industrial large-scale production. In addition, α LLL is not stable at room conditions by considering its melting point.

Talc addition led to a general reduction in crystallisation points of β, β' measured at cooling rates of 5-10°C/min whereas those of long-chain triglycerides (tripalmitin, tristearin) were not significantly affected. This could be ascribed to the occurrence of a more stable β' LLL. Talc appears to influence the solidification point of trilaurin, because adding 0.1% or 0.5% w/w, an increase in solidification point was observed. This implies lowered supercooling level, which might be in favour of nucleation. Addition of 1% w/w talc resulted in a decrease in melting point. This is controversary in comparison with documented data (Yoshikawa et al., 2015) but the cause could be the difference in granulometry of talc particles used. In fact, in the cited study, when mean size of talc particles increases to a critical value (2.5 µm), its effect on crystallisation point of trilaurin (cooled at 1°C/min) turned in reverse. It should be noticed that there might be also shear effect for homogeneous mixing brought about by a specification of 200 rpm in experiments.

Talc was used as an additive for it is a common excipient (glidant, lubricant) used in formulating solid dosage forms. Its effect on crystallisation of triglycerides and fat-based systems has been discovered recently (Bayés-García et al., 2022; Yoshikawa et al., 2014, 2015). By considering $T_{m,\beta}$ of pure LLL, the fact that talc-loaded formulations were shown to possess a relative β MSZW indicates evidently that talc can induce nucleation of β LLL. It is because this nucleation occurs above $T_{m,\beta'}$ of pure LLL. This highlights an advantage of the fact that construction of MSZW map by turbidimetry should be performed prior to another characterisation (e.g., DSC, optical microscopy).

Figure 4 also shows MZSW map constituted by melting and crystallisation points measured for all the trilaurin-based formulations where vitamin E TPGS was included as only or second additive. Though measurements of crystallisation points (5-10°C/min) were not performed, four regions could also be deduced. The importance was that addition of 10% w/w vitamin E TPGS did not also affect crystallisation of β LLL as indicated by the presence of a similar β MSZW.

In summary, sporadic crystallisation in β MSZW (region II) can yield a stable crystal form while formation of metastable form(s) likely results from spontaneous crystallisation below their melting points (region V). By showcasing the example of LLL, this signifies that each triglyceride in general can be adapted to at least two processing approaches depending on the level of thermal conditions in relation to the melting point of metastable form(s). From the overview of documented research with monoacid triglycerides, one melt-based processing technology could be more adapted to direct crystallisation of β polymorph than the other depending on their characteristics (e.g., mass and heat transfer mode, use of pressure, residence time). With the help of MSZW map as processability map, it can help select a transformation method with good thermal conditions, especially when additive addition or complex-mixture combinations are necessary, and even shun the use of high-capacity cooling unit. However, the dependence of other properties (e.g. solidification kinetics, adhesiveness, degradability of substrate) as function of temperature, additive quality and quantity should be also considered as they could influence processing performance.

2.3.2. Isothermal Crystallisation

2.3.2.1. Measurements of induction time and polymorph identification by DSC

Figure 5 shows solidification profile of the four selected formulations at 30°C during 2h (**A**) and polymorph identification after crystallisation (**B**). According to DSC results converted into solid fraction contents (%) as function of time (see **Figure 5-A**), four formulations LLL-1F, LLL-2F, LLL-3F and LLL-3F-1 (composition given in **Table 2**) exhibit an induction time of 751.2 s, 79.2 s, 14.4 s and 948.6 s, respectively. Solidification profile of four formulations can also be ranked as follows: LLL-3F > LLL-2F > LLL-1F > LLL-3F-1. According to DSC thermograms of four formulations as shown in **Figure 5-B**, all the formulations exhibit β form the melting point of which peaks at 48.2°C (LLL-1F), 50.9°C (LLL-2F), 49.0°C (LLL-3F) and 47.4°C (LLL-3F-1). Without talc, there is occurrence of β' and β'_1 forms indicated by peaks at 37.7°C and 43.6°C (LLL-1F), at 37.3°C and 42.8°C (LLL-3F-1), respectively (Hagemann, 1988). In the case of LLL-3F-1, the peak at 35.8°C is attributed to melting of vitamin E TPGS. Particularly, thermogram of LLL-3F also displays a peak of 41.5°C (black arrow) which could be attributed to either vitamin E TPGS or β'_1 form of trilaurin. For information, isothermal crystallisation of vitamin E TPGS at 30°C (data not shown) was also performed but there was no sign of thermal events during 2h. This characteristics should be noted for multi-sourced vitamin E TPGS as this semi-synthetic substance was reported to crystallise at this temperature upon continuous cooling (Li et al., 2011). The value of these melting peaks is higher than the reference value of trilaurin polymorphs because of a high heating rate of 30°C/min applied (Takeguchi et al., 2020; Yoshikawa et al., 2015).

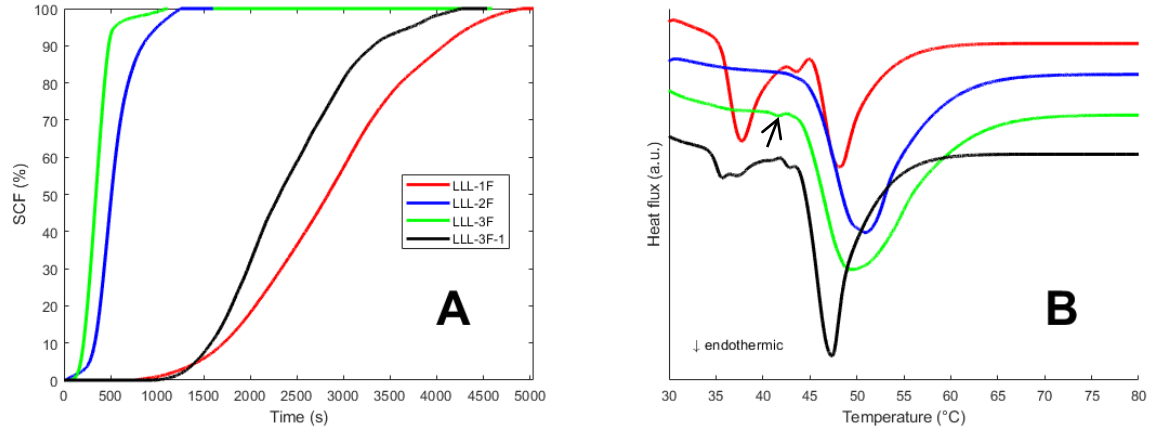

*Figure 5. Isothermal crystallisation of selected trilaurin-based formulations (A) and polymorphic identification of crystallised form(s) (B): LLL-1F (LLL**);*** LLL-2F (LLL+T 1.0%), LLL-3F (LLL+VitE_TPGS+T 1.0%), LLL-3F-1(LLL+VitE_TPGS).

Measurements of induction time via calorimetry yield a completely different landscape from those via turbidimetry (data not shown). In fact, talc addition results in the fact that induction time was reduced about 9.5 and 65.9 times for trilaurin and its combination with vitamin E TPGS. LLL-3F contains about 2.5%w/w talc and therefore the effect of talc addition on nucleation of LLL-3F might be magnified one order of magnitude in comparison with LLL-2F.

Another important aspect for melt processing is that the inclusion of talc accelerated solidification of trilaurin and its combination with vitamin E TPGS. In fact, slow solidification appears to be characteristics of β' form of triglycerides (e.g., trilaurin, tristearin) (Bertoni et al., 2021; Yoshikawa et al., 2015). In the presence of talc, β'- β conversion was catalysed and finished rapidly in the course of cooling (Yoshikawa et al., 2015). This justifies no observation of β' in polymorphic identification of LLL-2F and LLL-3F (see **Figure 5-B**).

In summary, in the presence of vitamin E TPGS, crystallisation behaviours of LLL-1F and LLL-3F-1 are similar in terms of polymorphic profile. In addition, when it comes to the case of LLL-3F-1, trilaurin seems to induce nucleation of vitamin E TPGS because the latter alone did not crystallise during an isothermal period of 2h at 30°C. With all the elements discussed, only LLL-1F, LLL-2F and LLL-3F were used as coating materials in this study where processing performance, coating quality, stability and release properties of coated products would be evaluated. LLL-3F-1 was characterised for comparison in terms of solidification properties as well as solid-state evolution with time.

2.3.2.1. Measurements of solidification time lag and film formation

Solidification behaviours of three trilaurin-based formulations used for hot-melt coating (LLL-1F, LLL-2F and LLL-3F) were investigated by means of goniometry. The main objective was to observe solidification and film formation in the case that primary or secondary nucleation takes place. The pictures taken over time (from deposition of a drop on the substrate's hot surface to solidification) can be seen in the ***Supplementary material (Figure S1)***. They demonstrate contact angle upon impingement, solidification, and film formation of LLL-1F, LLL-2F and LLL-3F on the surface of compressed NaCl and that of the formulation itself.

It could be observed that LLL-1F, LLL-2F and LLL-3F in molten state exhibit good wetting behaviours on the two substrates with a contact angle less than 90°. On this macroscopic scale, solidification time lag is considered as the time between the first contact (0 s) and the moment where the curve of the molten droplet started to deform. Solidification time lags of around 60 s, 60 s and 150 s were noticed for LLL-1F, LLL-2F and LLL-3F on NaCl surface and the solidification times were estimated to be about 240 s, 240 s and 300 s, respectively. On the other hand, the solidification process started about 30 s, 60 s and 30 s after its impact with the film of the same nature and finished within approximately 120 s, 240 s and 120 s, accordingly. At the end, all the solidified droplets display a rough surface but no sign of detachment on NaCl surface. This implies that trilaurin-based formulations have a good affinity to substrate.

In general, solidification of molten formulation on NaCl and on the surface of the same nature was homologous to primary nucleation and secondary nucleation, respectively. It is presumed that when solidification time lag of both nucleation phenomena approaches it is possible to set only one feeding rate instead of two as is applied to the case of tristearin (Lopes et al., 2015). Therefore, in this study, for all the coating trials, only one feeding rate was specified for the whole operation by considering also the solidification profile obtained for each formulation via DSC.

2.4. Process Performance and Coating Quality

2.4.1. Process Efficiency

For coating by fluidised bed, it is possible to generate products with different drug or coating contents in the same batch. This strategy was adopted as a multiple-sampling approach for HMC process and product characterisation.

Process yield for HMC with LLL-1F, LLL-2F and LLL-3F was recorded as 84%, 91% and 88%, accordingly. **Figure 6** shows coating contents of samples taken during each trial. In general, good yield and process efficiency were obtained with three formulations. Coating process efficiency observed for LLL-1F and LLL-3F, depicted by the red continuous line, approaches 100% at the end of operation but that of LLL-2F falls close to 80%. It could be also indicated by the gap between the theoretically calculated values (black filled squares) and the practical assay results (blue columns). In the case of LLL-1F and LLL-3F, assay of the samples 03 and end-R was found similar whereas results of LLL-2F display a difference. An explanation could be that at the moment of 3rd sampling a large amount of fine trilaurin was collected

and at the end of coating this fine fraction was segregated while coated particles were still in fluidisation.

This might be due to the propensity of trilaurin to generate fine. Actually, process data (not shown) indicates a continuous increase in filter pressure. All the coating operations lasted less than 6 minutes. For information, preliminary trials were performed with LLL-2F by augmenting feeding rate from 6-7, 11-12 to 18-19 g/min. At the final rate, fine powder was not observed evidently on the process wall. As trilaurin-containing formulations (LLL-1F and LLL-3F) exhibit a fast solidification kinetics, it is not advisable to specify a lower feeding rate. Otherwise, fine generation would be important.

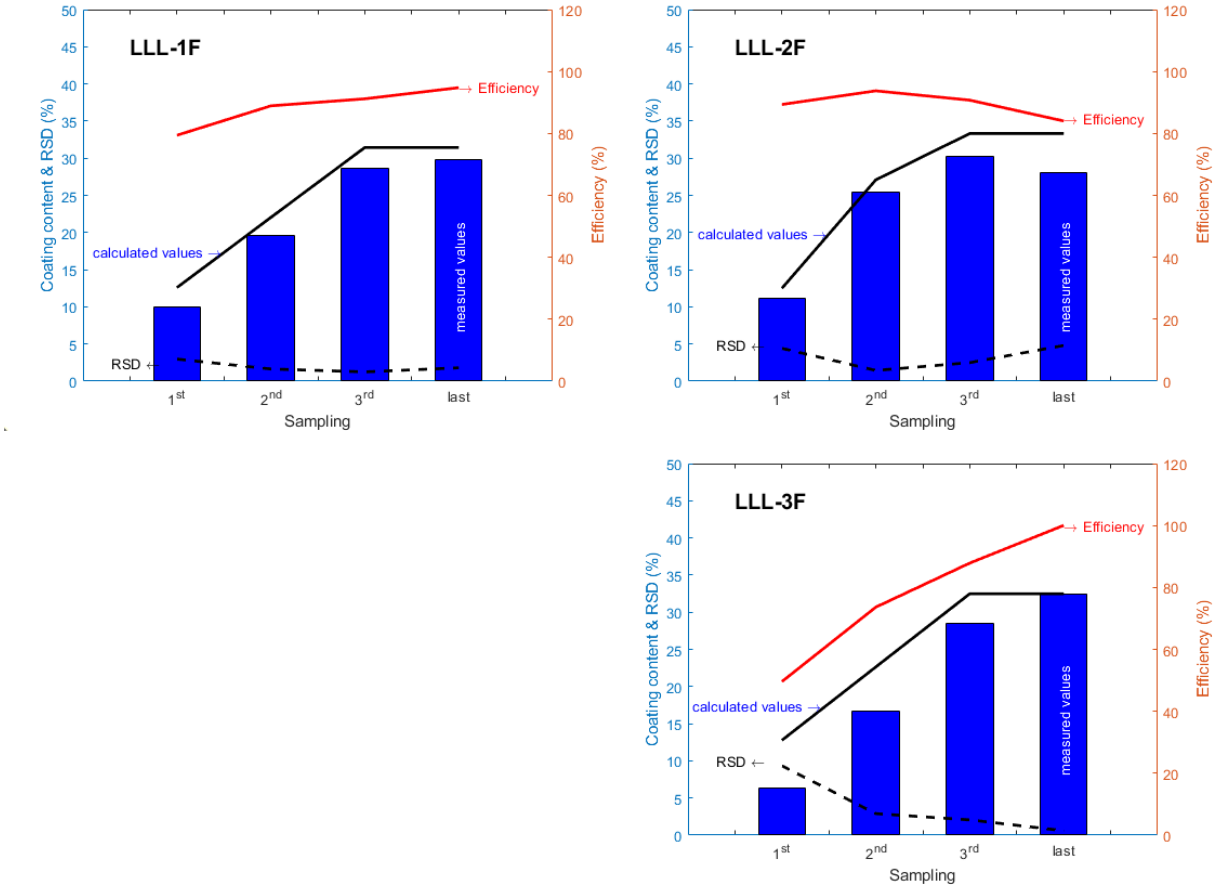

Figure 6. Assay results of coating trials performed with LLL-1F, LLL-2F and LLL-3F

2.4.2. Identification of Process Regime

The process regime could be determined by interpreting PSD and its parameters SPAN and $D_{v(90)}/D_{v(10)}$.

Figure 7 shows superimposed PSD curves expressed in volume (left) measured for initial NaCl particles, 1st, 2nd and 3rd sampling during coating trials corresponding with the three assayed coating contents in the previous section. Evolution of all the PSD curves indicates a progressive coating regime.

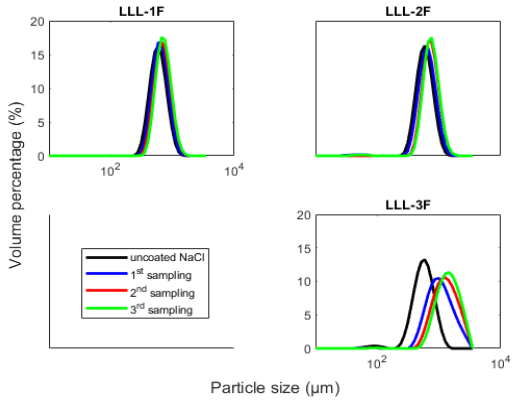

Product name		$D_{[4,3]}$ (µm)	$D_{[3,2]}$ (µm)	$D_{v(90)}/D_{v(10)}$	SPAN
Uncoated NaCl		649	595	2.05	0.75
LLL-1F	1st sampling	681	600	1.98	0.71
	2nd sampling	730	662	1.99	0.72
	3rd sampling	836	766	1.92	0.68
LLL-2F	1st sampling	707	570	2.17	0.88
	2nd sampling	811	748	1.94	0.69
	3rd sampling	820	695	1.94	0.74
LLL-3F	1st sampling	1210	918	3.42	1.36
	2nd sampling	1470	1160	3.19	1.23
	3rd sampling	1600	1320	2.93	1.12

Figure 7. Evolution of particle size distribution in volume (left) and PSD parameters (right) obtained for products coated with LLL-1F, LLL-2F and LLL-3F

As an exception, in the case of LLL-3F, the first PSD curve of 1st sampled particles display a reduced median peak but the trends reverse after that. This implies particles were agglomerated but then a strict coating regime was maintained. Initial agglomeration is probably the resultant of specifying one feeding rate for the whole agglomeration. This corroborates the hypothesis where it is possible to apply merely one feeding rate in the case of non-traditional coating (where temperature of fluidisation air > $T_{m,\alpha}$) when induction time of primary nucleation approaches that of secondary nucleation. It is not the case of LLL-3F. Measurements of solidification time with goniometry are rather appropriate for justifying a strategy to define process variables than DSC. In fact, LLL-3F and LLL-2F display both a similarly rapid solidification profile but this information appears irrelevant for setting a good feeding rate.

Besides, fine generation was observed for LLL-2F processed at the same thermal operational conditions as LLL-1F and LLL-3F. Fast solidification kinetics is likely the only cause. Measurements of solidification time and film formation demonstrated that all trilaurin-containing formulations adhere well to NaCl substrate and itself.

The evolution of PSD parameters SPAN and $D_{v(90)}/D_{v(10)}$, as given in **Figure 7** (right), is in accordance with the discussion on PSD curves. For LLL-1F and LLL-2F, constant decrease in both SPAN and $D_{v(90)}/D_{v(10)}$ indicates a progressive coating regime. However, in the case of LLL-3F, the initial jump from 2.05 $D_{v(90)}/D_{v(10)}$ of uncoated particles) to 3.42 ($D_{v(90)}/D_{v(10)}$ of 1st sampling) denotes a mixed regime of coating and agglomeration. These arguments agree with a hypothesis that when a coating regime dominates fine particles tend to gain more coating materials with time in comparison with larger particles, the width of PSD should reduce and the median peak $D_{v(50)}$ should sharpen. Otherwise, agglomeration leads to an enlargement of particle size and a rapid shift of PSD to greater class size bins.

Highest product temperature – 44.1°C, 46.4°C and 43.9°C – was noted for coating with LLL-1F, LLL-2F and LLL-3F, respectively. Despite its closeness to $T_{m,\beta}$, a strict coating regime with trilaurin-containing formulations was identified. This suggests that fast solidification induced by talc may be the contributing factor of the expected coating regime whereas slow solidification could cause agglomeration. Talc addition could be a key factor for successful non-traditional hot-melt coating with triglycerides.

2.4.3.Coating Quality

Coating quality of salt particles coated with LLL-1F, LLL-2F and LLL-3F was assessed visually using an optical microscope. **Figure 8** shows images salt particles uncoated and coated with increasing contents

of LLL-1F, LLL-2F, and LLL-3F, correspondingly. The length of the thick white bar indicates an observation scale of 200 µm. Uncoated salt particles had bright and almost translucent aspect, polygonal shape and rather sharp edges which were gradually rounded with coating. It should be noted that these observations were performed under the same lighting conditions. Reduction in brightness of salt crystals reflects increase in coating coverage. Fine particles less than 200 µm (orange circle) were detected among LLL-2F-coated particles, which was also observed in PSD. In the case of LLL-3F-coated particles, as discussed before (see **Section 2.4.2**), both coated and agglomerated particles could be observed, and the image of 1st sampling shows mostly agglomerates formed by two collided particles. These particles were still observed with a larger size in 2nd and 3rd sampled populations, which implies a strictly coating established after initial agglomeration. This agrees with considerations of process regime using PSD parameters (right on **Figure 7**).

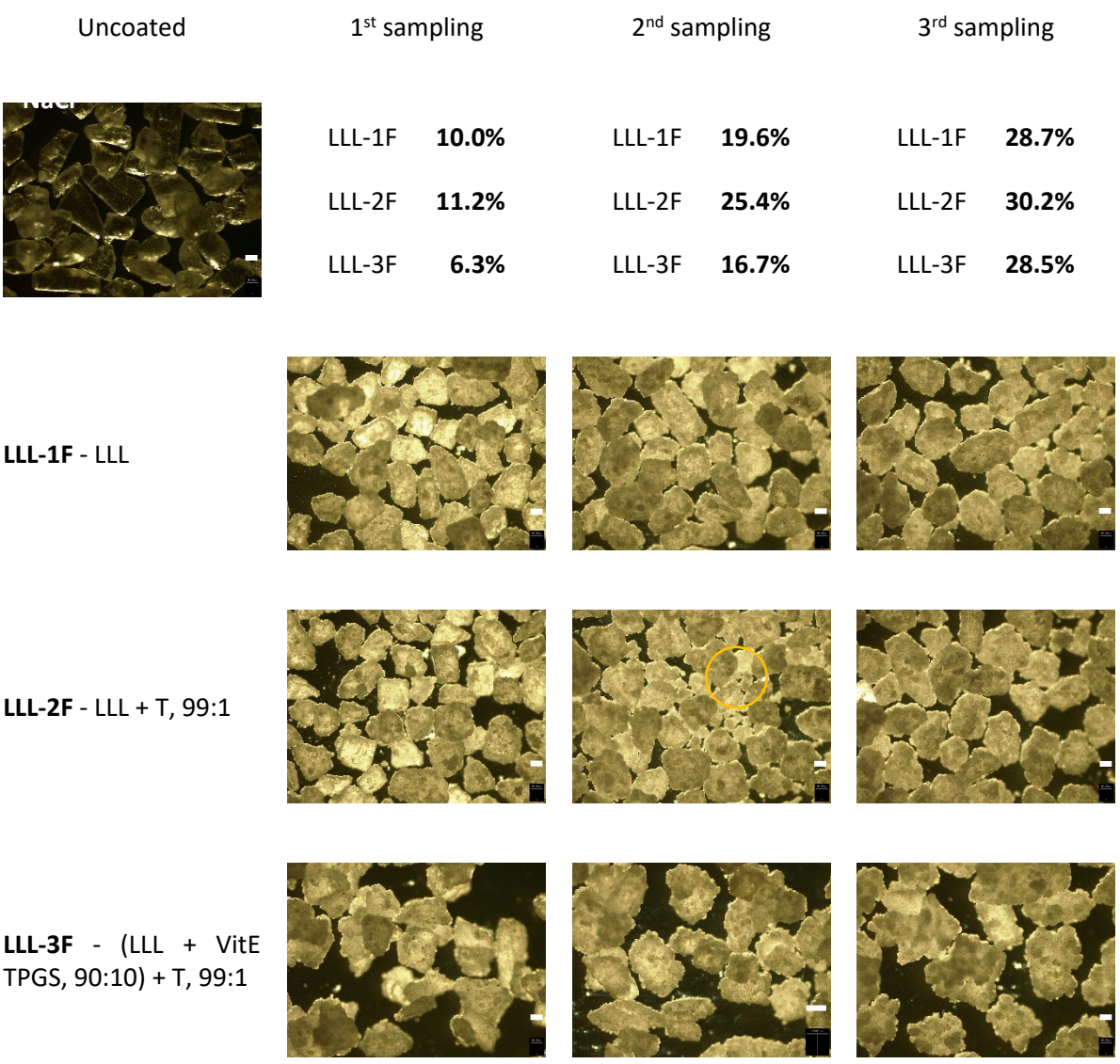

Figure 8. Optical images of salt particles uncoated and coated with LLL-1F, LLL-2F, and LLL-3F with increasing coating contents. The length of the thick white bar indicates an observation scale of 200 µm.

2.5. Release Properties and Product Stability

2.5.1. Polymorphism

Samples of products coated with the proposed lipid were evaluated at several timepoints: LLL-1F, LLL-2F and LLL-3F (03 timepoints): after production (t_0), after 6 weeks (t_1) and after 12 weeks (t_2). Samples were stored in freezer before analyses.

In **Figure 9** the thermograms of products coated with LLL-1F and LLL-2F display close melting points 48.6 and 48.3°C, respectively. This indicates that the crystallised form β was obtained after production (Kaneko et al., 2020; Lee et al., 2010). It should be noted that for trilaurin without talc, the crystallised form β' could be formed at the moment of production but at the time of analysis (more than 1 day of delay) β' was not stable enough in freezer and transformed completely into β (Windbergs et al., 2009b). In the case of LLL-3F, the thermogram has two melting peaks at 34.5°C (black arrow) and 47.5°C, which indicates solid-solid phase separation and depression in melting points of trilaurin.

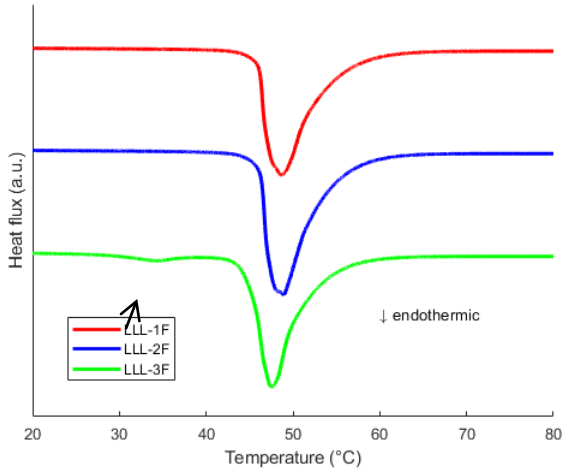

Figure 9. Polymorphic identification performed on products coated with LLL-1F, LLL-2F and LLL-3F at t_0

Figure 10- A1, A2, B1, B2, C1 and **C2** show small-angle and wide-angle XRPD patterns obtained for products coated with LLL-1F, LLL-2F and LLL-3F over three months, respectively. According to these XRPD patterns, long d-spacings of LLL-1F (**A1**), LLL-2F (**B1**) and LLL-3F (**C1**) were found between 31.2 and 31.8 Å (2.830-2.776° 2θ) and short d-spacings of LLL-1F (**A2**), LLL-2F (**B2**) and LLL-3F (**C2**) have the values of 4.6 Å (19.286-19.249° 2θ), 3.9 Å (23.196-23.023° 2θ) and 3.7 Å (23.978-23.720° 2θ). These long and short d-spacings correspond to β polymorph of trilaurin (Kaneko et al., 2020; Lee et al., 2010). With a chain of polyethylene in its structure, vitamin E TPGS alone seems to exhibit sub-α or β' packing (Li et al., 2011) and incorporate well with trilaurin crystal network. Hence, XRPD appears not capable to detect phase separation of vitamin E TPGS at 10% w/w.

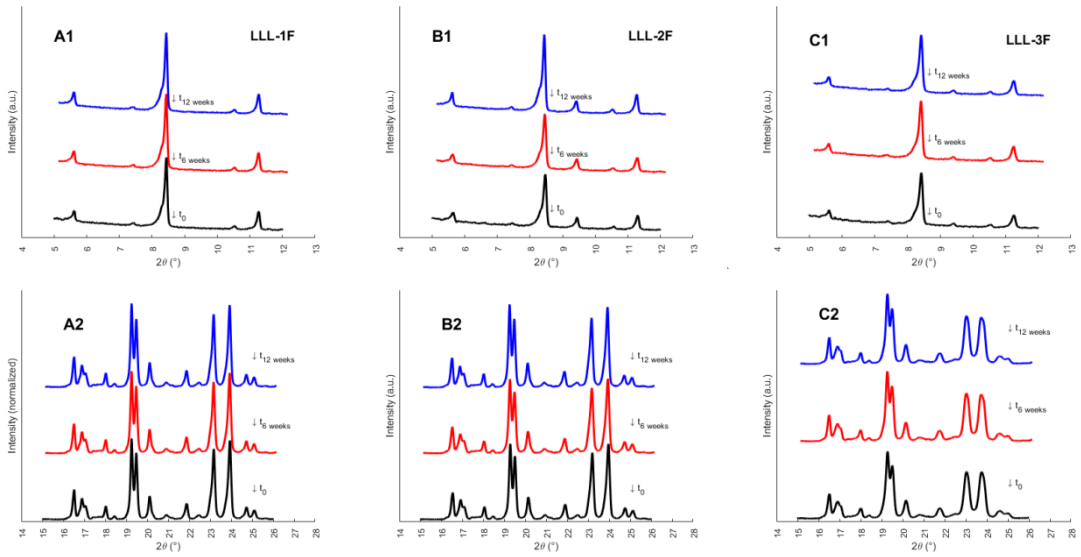

Figure 10. Small-angle (left) and wide-angle X-ray powder diffraction patterns obtained for products coated with LLL-1F, LLL-2F and LLL-3F at t_0 (black line), 6 weeks (red line) and 12 weeks (blue line) after t_0

2.5.2.Crystal Network and Phase Behaviours

Crystal network was evaluated based on monitoring crystallite size via XRPD analyses and polarised-light optical observations. **Table 5** shows estimated crystallite size and number of stacked lamellas measured for coated products with the ranking order of LLL-1F > LLL-2F > LLL-3F. Melting point of LLL-1F, LLL-2F and LLL-3F measured at t_0 appears to correlate with estimated crystallite size. In fact, melting point increases when estimated crystallite size increases as expected (Takeguchi et al., 2020). Without additive, crystal network of LLL-1F displays larger crystallite size than that of LLL-2F and LLL-3F formed under the effect of talc. This is in agreement with polarised light optical observations published in a research on talc (Yoshikawa et al., 2014).

Table 5. Estimated crystallite size and number of stacked lamellas

Formulation		Crystallite size (Å)	Stacking no. of lamellas#
LLL-1F	**t_0**	1597	50.7
	t_1	1613	51.2
	t_2	1726	54.8
LLL-2F	**t_0**	1205	38.3
	t_1	1205	38.3
	t_2	1435	45.6

LLL-3F	t_0	979	31.1
	t_1	1166	37.0
	t_2	1190	37.8

[#]Rounded values were shown.

Polarised light optical images performed in-house with LLL-1F, LLL-2F, LLL-3F and LLL-3F-1 will be discussed in the following. **Figure 11** shows in parallel representative polarised light optical images of LLL-1F and LLL-2F taken in intervals of 6 weeks. The samples were kept in lamellas and preserved hermetically at 25°C/60% relative humidity. LLL-1F at the time of formation (t_0) was constituted of large spherulite crystals (Yoshikawa et al., 2014). Both images taken at 6 weeks and 12 weeks (LLL-1F) show that such spherulite crystals were transformed into β in the form of small loosely packed crystals. In the case of LLL-2F, images taken at t_0, 6 weeks and 12 weeks display crystal morphology characterised for β and not changed significantly with time : spherulites with strong birefringent patterns (Oh et al., 2002; Yoshikawa et al., 2014).

t_0 t_1 (6 weeks) t_2 (12 weeks)

LLL-1F

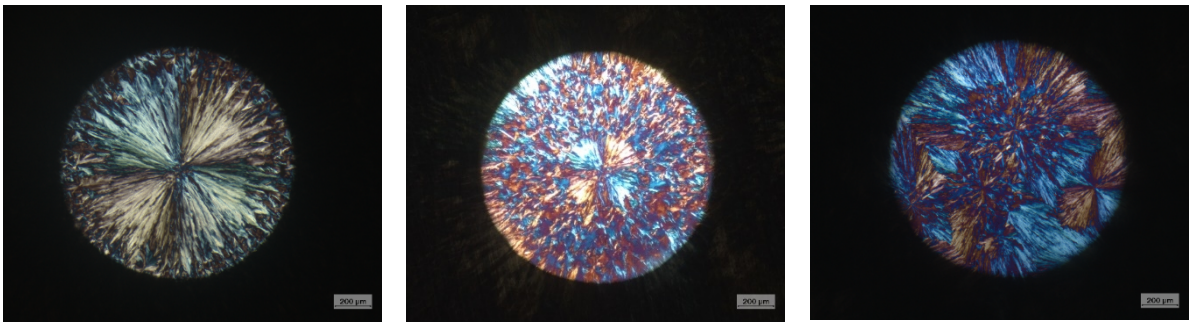

LLL-2F

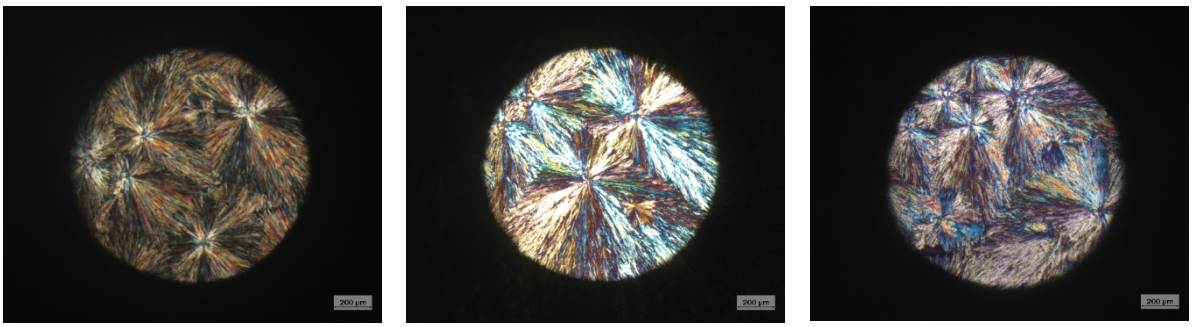

Figure 11. Polarised light optical images performed for LLL-1F, LLL-2F at t_0, 6 and 12 weeks after t_0 (length of the bar is 200 µm).

Figure 12 shows in parallel representative polarised light optical images of LLL-3F and LLL-3F-1 taken in intervals of 6 weeks. **Figure 12** also shows polarised light optical images of vitamin E TPGS crystallised at room conditions (not at 30°C). They show large crystallites stack one on top of another. Crystallite size also seems not to evolve with time. The observations of vitamin E TPGS were performed to complement those of LLL-3F and LLL-3F-1. Back to sample LLL-3F-1, its optical image at (t_0) appears to display hybrid features of large spherulites β' and β and large crystallites of vitamin E TPGS without net borders. After 6 weeks, de-mixing of vitamin E TPGS was detected easily like its morphology observed in **Figure 12.** After 12 weeks, appearance of spherulites of vitamin E TPGS could be indicative of net phase separation between two components of the system. The crystal network of β LLL-3F (t0) also comprised of spherulites with birefringent patterns. There seems not to be significant changes in crystal morphology at 6 weeks and 12 weeks. At the last timepoints, a small piece of vitamin E TPGS like crystals could be also observed.

t_0	t_1 (6 weeks)	t_2 (12 weeks)

Vitamin E TPGS

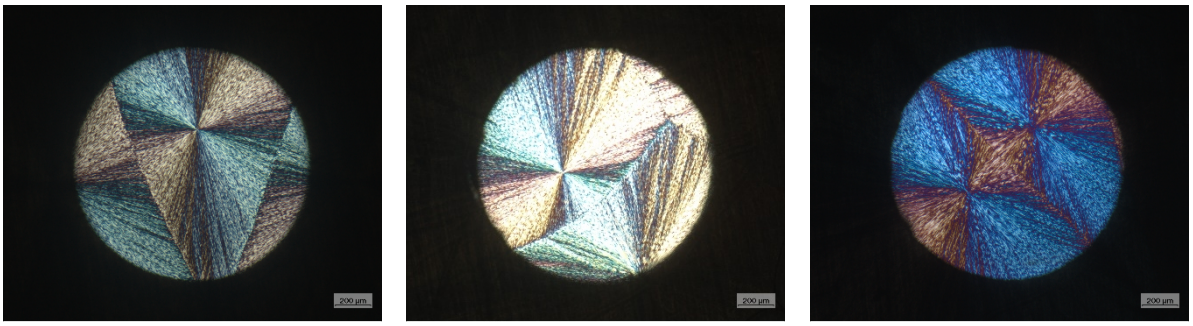

LLL-3F

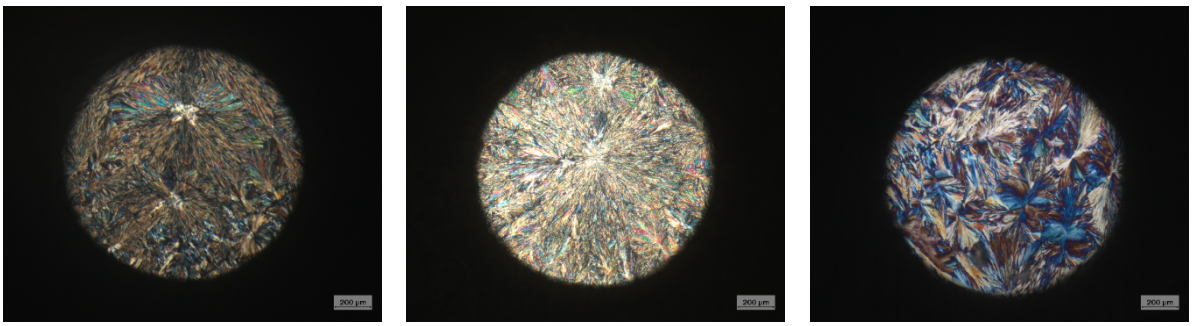

LLL-3F-1

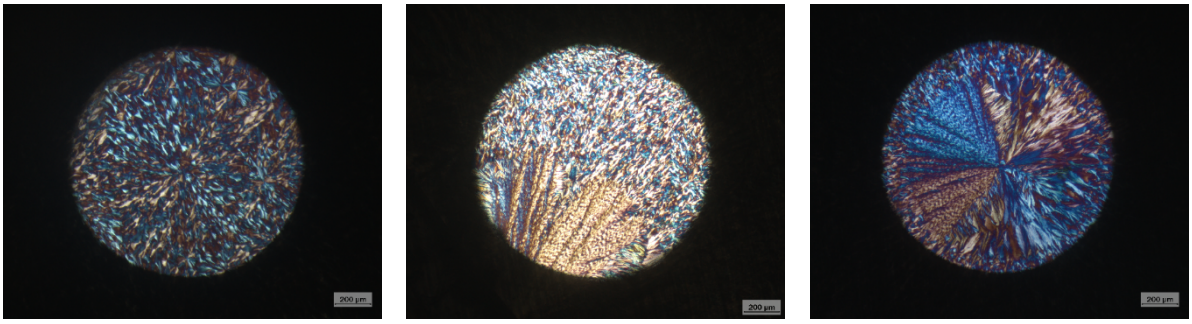

Figure 12. Polarised light optical images performed for vitamin E TPGS, LLL-3F and LLL-3F-1 at t_0, 6 and 12 weeks after t_0 (length of the scale bar is 200 µm)

These observations show at least two advantages of formulating trilaurin and vitamin E TPGS with talc. On the one side, talc promoted an even crystal network populated with β polymorph spherulites the size of which seems not to change significantly over three months. On the other side, fast solidification kinetics of β form appears to trap vitamin E TPGS which crystallised under the effect of trilaurin. Therefore, despite the immiscibility of two components at the ratio 90:10, phase separation could be overcome via fast crystallisation induced by talc. The whole crystallisation of the ternary formulation, composed of trilaurin, vitamin E TPGS and talc, (90:10), 99:1 was recorded as evidence (data not shown).

2.5.3.Hygroscopicity Profile

As trilaurin is water-resistant and formulating with additives could modify its property, salt particles coated with trilaurin-based formulations were tested with dynamic vapour sorption with the objective of (i) monitoring any physical changes when these products were subject to aging at 25°C/60% relative humidity and (ii) testing a technological functionality, i.e. moisture-proofing property of each formulation.

Figure 13 shows the results of dynamic vapour sorption obtained for NaCl and its products coated LLL-1F, LLL-2F and LLL-3F. The sorption curves show evidently that at some moisture increments of 10% to 95% change in mass (%) had not attain its most because of insufficient equilibrium time set for each step. In fact, as a humidity regulating agent, NaCl can absorb 10-100 times higher its mass and experimentation could be long-lasting (Sängerlaub et al., 2018). Therefore, provided that the same protocol was applied, the results should be comparable.

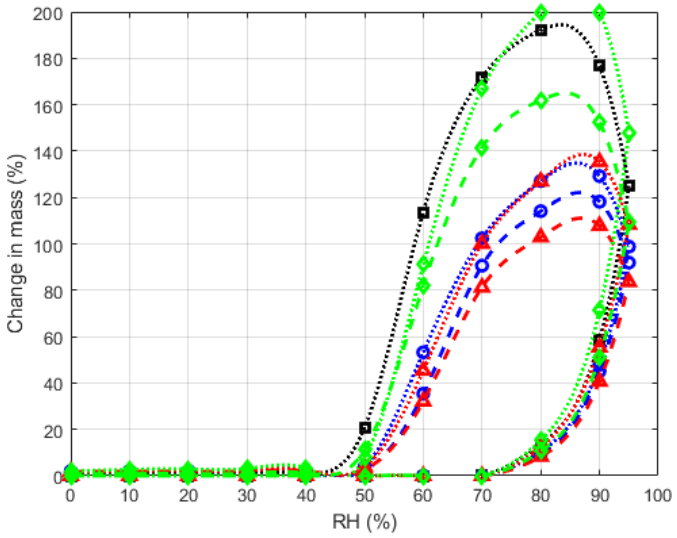

Figure 13. Dynamic vapour sorption profile obtained for uncoated NaCl and products coated with LLL-1F, LLL-2F and LLL-3F at t_0 and 12 weeks after that; uncoated NaCl (black open square), LLL-1F (blue open circle), LLL-2F (red open triangle), LLL-3F (green open diamond), measurements at t_0 (dotted lines) and at 12 weeks after that (dashed lines)

All the samples start to absorb vapour above 70% relative humidity which is near the deliquescence point of NaCl (Sängerlaub et al., 2018). Both uncoated NaCl and LLL-3F-coated products (t_0) exhibit the highest vapour sorption kinetics with a peak up to 2 times change in mass. This implies that vapour absorbed would dissolve both NaCl and vitamin E TPGS occurring in the products. Without inclusion of the hydrophilic surfactant LLL-1F- and LLL-2F-coated products have a similar and milder vapour sorption kinetics which attain its peak at about 1.4 times change in mass. For all the cases, desorption process was faster for coated products than uncoated NaCl.

After 3 months of storage, all the coated products exhibit lower vapour sorption kinetics with the ranking order of LLL-2F < LLL-1F < LLL-3F. Reduced in sorption kinetics after three months suggests that the coating quality in terms of surface and microstructure could evolve. This observation is in agreements with the increase in estimated crystallite size during storage. In fact, fat blooms (or continuous crystal growth on surface) often happen to lipid-based products and trilaurin-based formulations could not be exempt from this physical process. There have been reports of triglycerides affected by fat blooming (Bertoni et al., 2021; Mayama, 2009; Witzleb et al., 2012). When blooms are developed, normally the surface will become more water-repellent (Fang et al., 2007) and release kinetics of active substance could therefore decelerate.

In practice, sorption isotherms have been interpreted to evaluate moisture-proofing of the hot-melt coat (Achanta et al., 2001; Chen et al., 2010). In this case, moisture-proofing property of bloomed lipid-coated salt could be deemed improved in comparison with t_0. However, it is advisable to coat with trilaurin without hydrophilic additive if the applications of its formulations were for moisture protection.

2.5.4.Release Properties

Measurements of salt release kinetics not only reflect the impact of solid-state evolution on performance stability. As NaCl crystals represent a simple active model, it can also help verify susceptibility of formulations in development to phase separation, which has been reported to cause release instability of lipid-based formulated products (Lopes et al., 2017). **Figure 13** demonstrates comparative release profile of salt particles coated with LLL-1F, LLL-2F, and LLL-3F during a stability

period of three months. For LLL-1F and LLL-2F, a prolonged release was obtained. Qualitatively, salt was released from LLL-1F- or LLL-2F-formulated products to similar rate and extent at t_0 and 12 weeks. Salt release was observed to decelerate between these two timepoints. This could be probably due to growth of crystallite size and fat blooming (Schertel et al., 2021; Witzleb et al., 2012). In the case of LLL-3F, it imparts an immediate release (i.e. more than 85% dissolved within 30 min) to salt coated with a similar content. The incorporation of vitamin E TPGS might create hydrophilic channels that facilitates in turn water transfer throughout lipid coat.

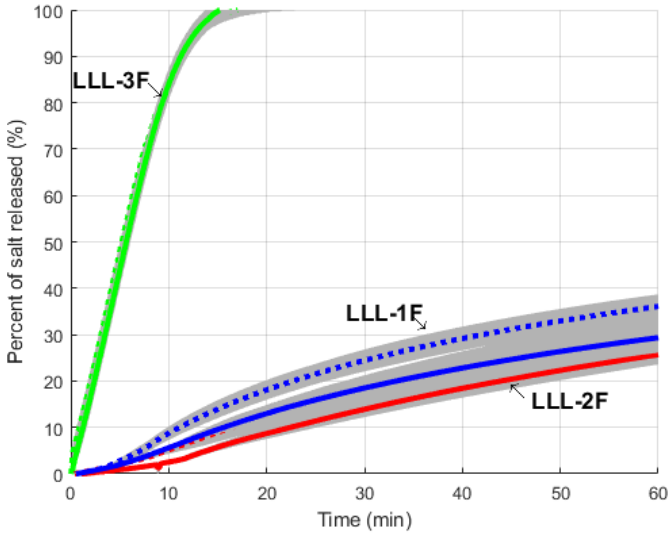

Figure 14. Salt release profile obtained for products coated with LLL-1F (red), LLL-2F (blue) and LLL-3F (green) at t_0 (dotted lines) and 12 weeks (solid lines) after that. Error bar (grey region)

Notably, release profile of salt coated with LLL-3F appears not to change over three months despite initial phase separation and continuous evolution of its solid-state behaviours. On the one hand, in spite of phase immiscibility of vitamin E TPGS at 10% w/w, this component could also crystallise at the time the crystal network of trilaurin formed and was found to be evenly dispersed therein. In other words, it is reasonable to state that there formed a non-solid solution system where mobility of solid vitamin E TPGS was minimised. As discussed before, trilaurin acts as a crystallisation inductor for vitamin E TPGS (See **Section 2.3.2.1**) while talc acts as a promoter of both nucleation and crystal growth for trilaurin (See **Section 2.5.2**).

From a quantitative perspective, two-sample t-test confirms that there is no significant difference (α = 5%) in salt release kinetics between t_0 and 6 weeks, between 6 weeks and 12 weeks for all the three formulations. f_2 factor test could be more discriminative but it necessitates a larger number of tested samples.

2.5.4.1. Digestibility

Trilaurin is a medium chain triglyceride (Jadhav & Annapure, 2023) but its digestibility sometimes goes unnoticed when formulating solid lipid formulations (Windbergs et al., 2009d, 2009c, 2009a). The products coated with LLL-1F, LLL-2F and LLL-3F were then tested with a focus on the digestibility of these formulations.

Figure 15-A shows digestion kinetics of the three trilaurin-based formulations. In this graph, digestion kinetics is indicated by the rate of NaOH consumption. As can be seen, LLL-1F and LLL-2F appear to be digested to the similar rate during the whole experiments. It implies that talc 1% w/w has no significant effect on digestion of trilaurin. In the case of LLL-3F, digestion was slow at beginning in comparison

with LLL-1F and LLL-2F but after 150 min its digestion rate reached that of those two formulations. As shown in **Figure 15-B**, both digestion extents (%) determined via direct titration and back titration were close, showing that at 3h all the three formulations were digested to the similar extent. Addition of vitamin E TPGS changed the digestion mechanism of the formulation at the beginning, but its digestion extent is equivalent to trilaurin after 3h.

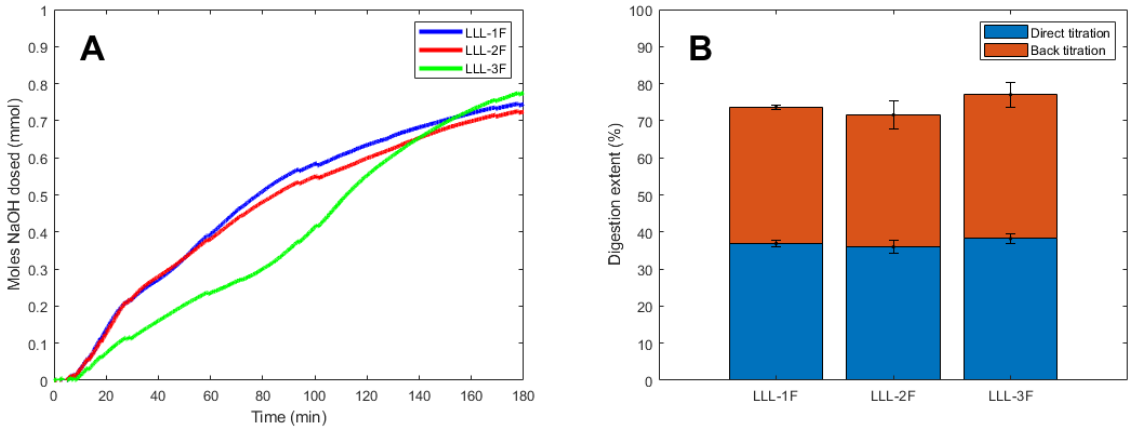

Figure 15. Digestion profile of 500 mg each formulation LLL-1F, LLL-2F and LLL-3F (t_0)

Following a normal mechanism of triglyceride digestion, a triglyceride is firstly attacked by lipase, at positions sn-1 and sn-3, to produce one fatty acid and one 1,2-diacylglyceride. The latter is then cleaved by lipase to yield one fatty acid and 2-monoglyceride. The latter should be then converted to 1-monoglyceride so that lipase could hydrolyse it into one fatty acid and one glycerol (Benito-Gallo et al., 2015; Jensen et al., 1963). The difference in digestion kinetics is indubitably due to the presence of vitamin E TPGS which is not digestible but known to inhibit lipolysis to some extent (Christiansen et al., 2010). It was reported to mimic binding of co-lipase and thereby blocking the association of co-lipase with pancreatic lipase but different mechanisms were also suggested (Christiansen et al., 2010). As a hypothesis, vitamin E TPGS could compete with pancreatic lipase at the beginning, and this resulted in retarded digestion kinetics. In the course of lipolysis, more digestion products were generated and they might have a more or less affinity with vitamin E TPGS to form solubilising structures (Jensen et al., 1963). This should progressively free up the enzymes' active sites. Furthermore, at this point, almost trilaurin should have been digested into digestion products. The more they are solubilised, the faster they could be digested (Christophersen et al., 2013; Witzleb et al., 2012).

The quantity of each sample was normalised to 500 mg of each formulation. To compare digestibility of different liquid lipid types, the tests could be performed on the same quantity of lipids with all the same parameters (Arnold et al., 2012). To compare digestibility of different solid lipid types or formulations, total surface area of solid systems should be considered as an important factor (Vithani et al., 2019). As is demonstrated in this case study, use of coated microparticulate systems could be a viable suggestion for this type of comparative study. In fact, digestion of monolithic systems was also tested but a digestion extent obtained at the end of 3h was neglectable in comparison with that of multiparticulate systems (data not shown).

Previous studies performed on lipid digestibility (Bertoni et al., 2018, Christophersen, Vaghela, et al., 2014; Christophersen, Zhang, et al., 2014) also agree that system size is important for designing a comparative study of lipid digestibility.

2.5.4.2. *Effect of Digestion*

When it comes to solid lipid-based formulations, release testing in biologically simulated media in the presence of lipolytic enzymes has been sparsely conducted. **Figure 16** shows the results of release testing coupled with *in vitro* lipolysis which was performed on three types of coated products. The graph shows that for all the coated products an immediate release profile, i.e. at least 85% active substance released within 45 min (Siewert et al., 2003) could be obtained instead of an extended release profile for LLL-1F and LLL-2F when performing release testing without lipolysis. Therefore, it is important for testing solid lipid-based formulated products that release testing coupled with *in vitro* lipolysis should be performed. As discussed before (see **Section 2.5.4**), release testing in water is always, though, practical, and vital for evaluation of quality in batch release and long-term stability.

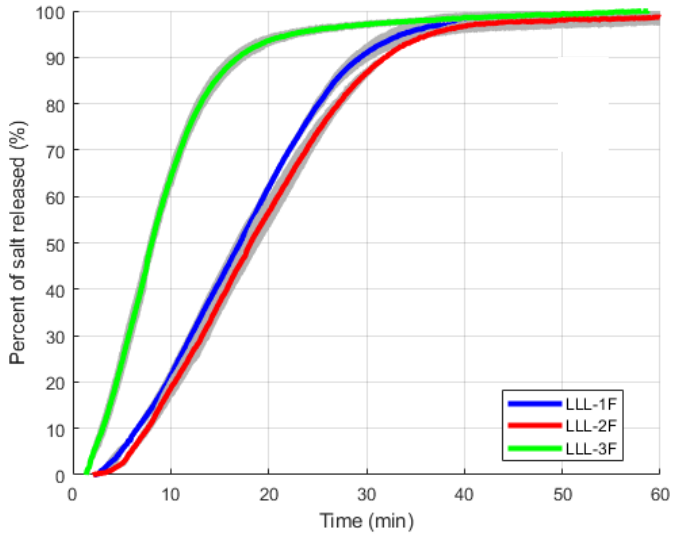

Figure 16. Salt release profile of products coated with LLL-1F, LLL-2F and LLL-3F subject to lipolysis

3. CONCLUSIONS

To exploit lipids for their functionalities (e.g., taste-masking, enteric coating, prolonged release), it is of utmost importance to overcome processability and stability issues. All the development work performed in this work is till this point to highlight trilaurin – a neglected medium-chain triglyceride – which could be used in hot-melt coating for several projective applications (e.g. moisture-proofing, taste-masking).

As fat in general, triglycerides in particular and notably trilaurin are likely to be substrate of *in vivo* lipolysis, combination of dissolution and digestion should become a normal testing for solid lipid-based formulated products in order to explore a full landscape of their functionalities.

Concerning the effect of composition of trilaurin-based coat formulations, this research work demonstrates the effect of talc and vitamin E TPGS on manufacturability, release properties and stability of products hot-melt coated with trilaurin-containing formulations. Firstly, as showcased by the study of trilaurin, for saturated monoacid triglycerides whose polymorphic profile comprises different polymorphs, two melt-based processing approaches are possible according to the choice of either β MSZW (II) or thermal conditions less than $T_{m,\alpha}$ (IV or V). This highlights the impact of additives on processability of solid lipid-based formulations as well as adds more values to already developed triglyceride-based formulas. Secondly, with technical feasibility proof for the addition of vitamin E TPGS, its combination with trilaurin and talc was chosen for hot-melt coating compared to trilaurin without/with talc. There is a link between solidification properties of these formulations, specification

of process variables and processing performance. Thirdly, the advantages of non-conventional hot-melt coating are guaranteed as a stable polymorphic profile obtained after production with no need for curing. Despite the evolution of solid-state behaviours, a new strategy to improve release stability of lipid-based formulated products was revealed: fast crystallisation of trilaurin-based formulations induced by talc. In fact, though phase separation for the ternary combination was observed from the beginning, salt release kinetics was found relatively stable with time.

Last but not least, coating with these formulations imparted a lower humidity sorption in comparison with uncoated NaCl. Addition of talc 1% w/w or vitamin E TPGS 10% w/w did not significantly influence the digestibility of trilaurin at the end of 3h lipolysis. As expected, digestion of trilaurin with a coating content around 30% w/w results in an immediate release profile for trilaurin and its binary combination. In conclusion, the results of this case study highlight the fact that a thorough understanding of material properties (e.g. crystallisation, polymorphism, digestibility) is of utmost importance for melt-processing, stabilising, and customising release profile of solid lipid-formulated products.

4. SUPPLEMENTARY MATERIALS

Supplementary information – Observations of solidification & film formation of a molten droplet of formulation deposited on surface of NaCl or formulation itself at 30°C.

5. ACKNOWLEDGEMENTS

This work was produced in the framework of a thesis financed by Occitanie region, Castres-Mazamet joint research association with a contribution from SEPPIC. The authors also thank the teams of technicians and engineers at IMT Mines Albi for their technical support (L. Haurie, A. Perron, A. Lafon, L. Devriendt, M. Chambard, S. Patry, P. Acart, V. Nallet, S. d Confetto, C. Rolland and K. Viellevigne) and research team at University of Clermont Auvergne (S. Denis, S. Chalancon, and C. Mazal).

6. DECLARATION OF INTEREST CONFLICTS

The authors declare no conflict of interest.

7. REFERENCES

Achanta, A. S., Adusumilli, P. S., James, K. W., & Rhodes, C. T. (2001). Hot-Melt Coating : Water Sorption Behavior of Excipient Films. *Drug Development and Industrial Pharmacy*, *27*(3), 241-250. https://doi.org/10.1081/DDC-100000242

Appelgren, C., & Eskilson, C. (1993). Size enlargement and coating by the use of melts. In *Industrial Aspects of Pharmaceutics*. Swedish Pharmaceutical Press.

Arnold, Y. E., Imanidis, G., & Kuentz, M. (2012). In vitro digestion kinetics of excipients for lipid-based drug delivery and introduction of a relative lipolysis half life. *Drug development and industrial pharmacy*, *38*(10), 1262-1269.

Aronhime, J. S., Sarig, S., & Garti, N. (1988). Dynamic control of polymorphic transformation in triglycerides by surfactants : The button syndrome. *Journal of the American Oil Chemists' Society*, *65*(7), 1144-1150.

Bayés-García, L., Yoshikawa, S., Aguilar-Jiménez, M., Ishibashi, C., Ueno, S., & Calvet, T. (2022). Heterogeneous Nucleation Effects of Talc Particles on Polymorphic Crystallization of Cocoa Butter. *Crystal Growth & Design*, *22*(1), 213-227. https://doi.org/10.1021/acs.cgd.1c00859

Beaupere, N., Soupremanien, U., & Zalewski, L. (2018). Nucleation triggering methods in supercooled phase change materials (PCM), a review. *Thermochimica Acta*, *670*, 184-201. https://doi.org/10.1016/j.tca.2018.10.009

Becker, K., Salar-Behzadi, S., & Zimmer, A. (2015). Solvent-free melting techniques for the preparation of lipid-based solid oral formulations. *Pharmaceutical research*, *32*(5), 1519-1545.

Benito-Gallo, P., Franceschetto, A., Wong, J. C. M., Marlow, M., Zann, V., Scholes, P., & Gershkovich, P. (2015). Chain length affects pancreatic lipase activity and the extent and pH–time profile of triglyceride lipolysis. *European Journal of Pharmaceutics and Biopharmaceutics*, *93*, 353-362. https://doi.org/10.1016/j.ejpb.2015.04.027

Bertoni, S., Passerini, N., & Albertini, B. (2021). Liquid Lipids Act as Polymorphic Modifiers of Tristearin-Based Formulations Produced by Melting Technologies. *Pharmaceutics*, *13*(7), 1089.

Brodkorb, A., Egger, L., Alminger, M., Alvito, P., Assunção, R., Ballance, S., Bohn, T., Bourlieu-Lacanal, C., Boutrou, R., Carrière, F., Clemente, A., Corredig, M., Dupont, D., Dufour, C., Edwards, C., Golding, M., Karakaya, S., Kirkhus, B., Le Feunteun, S., … Recio, I. (2019). INFOGEST static in vitro simulation of gastrointestinal food digestion. *Nature Protocols*, *14*(4), 991-1014. https://doi.org/10.1038/s41596-018-0119-1

Chen, H., Shi, S., Liu, A., & Tang, X. (2010). Combined application of extrusion-spheronization and hot-melt coating technologies for improving moisture-proofing of herbal extracts. *Journal of pharmaceutical sciences*, *99*(5), 2444-2454.

Christiansen, A., Backensfeld, T., & Weitschies, W. (2010). Effects of non-ionic surfactants on in vitro triglyceride digestion and their susceptibility to digestion by pancreatic enzymes. *European Journal of Pharmaceutical Sciences*, *41*(2), 376-382. https://doi.org/10.1016/j.ejps.2010.07.005

Christophersen, P. C., Vaghela, D., Müllertz, A., Yang, M., Nielsen, H. M., & Mu, H. (2014). Solid lipid particles for oral delivery of peptide and protein drugs III—the effect of fed state conditions on the in vitro release and degradation of desmopressin. *The AAPS journal*, *16*(4), 875-883.

Christophersen, P. C., Zhang, L., Müllertz, A., Nielsen, H. M., Yang, M., & Mu, H. (2014). Solid lipid particles for oral delivery of peptide and protein drugs II–the digestion of trilaurin protects desmopressin from proteolytic degradation. *Pharmaceutical research*, *31*(9), 2420-2428.

Christophersen, P. C., Zhang, L., Yang, M., Nielsen, H. M., Müllertz, A., & Mu, H. (2013). Solid lipid particles for oral delivery of peptide and protein drugs I–Elucidating the release mechanism of lysozyme during lipolysis. *European Journal of Pharmaceutics and Biopharmaceutics*, *85*(3), 473-480.

Clarkson, E. M., Curtis, J. R., Jewkes, R. J., Jones, B. E., Luck, V. A., De Wardener, H. E., & Phillips, N. (1971). Slow sodium : An oral slowly released sodium chloride preparation. *Br Med J*, *3*(5775), Article 5775.

Fang, W., Mayama, H., & Tsujii, K. (2007). Spontaneous formation of fractal structures on triglyceride surfaces with reference to their super water-repellent properties. *The Journal of Physical Chemistry B*, *111*(3), 564-571.

Feeney, O. M., Crum, M. F., McEvoy, C. L., Trevaskis, N. L., Williams, H. D., Pouton, C. W., Charman, W. N., Bergström, C. A., & Porter, C. J. (2016). 50 years of oral lipid-based formulations : Provenance, progress and future perspectives. *Advanced drug delivery reviews*, *101*, 167-194.

Frenning, G., Tunón, Å., & Alderborn, G. (2003). Modelling of drug release from coated granular pellets. *Journal of Controlled Release*, *92*(1-2), 113-123. https://doi.org/10.1016/S0168-3659(03)00300-6

Hagemann, J. W. (1988). Thermal behavior and polymorphism of acylglycerides. In *Crystallization and polymorphism of fats and fatty acids* (Vol. 31, p. 9-95). Marcel Dekker New York.

Jadhav, H. B., & Annapure, U. S. (2023). Triglycerides of medium-chain fatty acids : A concise review. *Journal of Food Science and Technology*, *60*(8), 2143-2152. https://doi.org/10.1007/s13197-022-05499-w

Jannin, V., & Cuppok, Y. (2013). Hot-melt coating with lipid excipients. *International journal of pharmaceutics*, *457*(2), 480-487.

Jensen, R. G., Sampugna, J., Parry Jr, R. M., & Shahani, K. M. (1963). Lipolysis of Laurate Glycerides by Pancreatic and Milk Lipase. *Journal of Dairy Science*, *46*(9), 907-910.

Kaneko, F., Yamamoto, Y., & Yoshikawa, S. (2020). Structural study on fat crystallization process heterogeneously induced by graphite surfaces. *Molecules*, *25*(20), 4786.

Kellens, M., Meeussen, W., Hammersley, A., & Reynaers, H. (1991). Synchrotron radiation investigations of the polymorphic transitions in saturated monoacid triglycerides. Part 2 : Polymorphism study of a 50:50 mixture of tripalmitin and tristearin during crystallization and melting. *Chemistry and Physics of Lipids*, *58*(1-2), 145-158. https://doi.org/10.1016/0009-3084(91)90120-Z

Kulkarni, S. A., Kadam, S. S., Meekes, H., Stankiewicz, A. I., & Ter Horst, J. H. (2013). Crystal Nucleation Kinetics from Induction Times and Metastable Zone Widths. *Crystal Growth & Design*, *13*(6), 2435-2440. https://doi.org/10.1021/cg400139t

Lee, Y. L., Ristic, R. I., DeMatos, L. L., & Martin, C. M. (2010). Crystallisation Pathways of Polymorphic Triacylglycerols Induced by Mechanical Energy. *Journal of Physics: Conference Series*, *247*, 012049. https://doi.org/10.1088/1742-6596/247/1/012049

Li, J., Yang, B., Levons, J., Pinnamaneni, S., & Raghavan, K. (2011). Phase behavior of TPGS–PEG400/1450 systems and their application to liquid formulation : A formulation platform approach. *Journal of Pharmaceutical Sciences*, *100*(11), 4907-4921. https://doi.org/10.1002/jps.22659

Lopes, D. G., Becker, K., Stehr, M., Lochmann, D., Haack, D., Zimmer, A., & Salar-Behzadi, S. (2015). Role of Lipid Blooming and Crystallite Size in the Performance of Highly Soluble Drug-Loaded Microcapsules. *Journal of Pharmaceutical Sciences*, *104*(12), 4257-4265. https://doi.org/10.1002/jps.24660

Lopes, D. G., Koutsamanis, I., Becker, K., Scheibelhofer, O., Laggner, P., Haack, D., Stehr, M., Zimmer, A., & Salar-Behzadi, S. (2017). Microphase separation in solid lipid dosage forms as the cause of drug release instability. *International journal of pharmaceutics*, *517*(1-2), 403-412.

Mayama, H. (2009). Blooming theory of tristearin. *Soft matter*, *5*(4), 856-859.

Moorthy, A. S. (2018). Melting and Solidification of Fats. In *Structure-Function Analysis of Edible Fats* (p. 101-118). Elsevier. https://doi.org/10.1016/B978-0-12-814041-3.00004-6

Müller, M. G., Lindner, J. A., Briesen, H., Sommer, K., & Foerst, P. (2018). On the properties and application of beeswax, carnauba wax and palm fat mixtures for hot melt coating in fluidized beds. *Advanced Powder Technology*, *29*(3), 781-788.

Nishihata, T., Yoshitomi, H., & Higuchi, T. (2011). Intestinal absorption of sodium cefoxitin in rats : Effect of formulation. *Journal of Pharmacy and Pharmacology*, *38*(1), 69-70. https://doi.org/10.1111/j.2042-7158.1986.tb04472.x

Oh, J.-H., McCurdy, A. R., Clark, S., & Swanson, B. G. (2002). Characterization and thermal stability of polymorphic forms of synthesized tristearin. *Journal of food science*, *67*(8), 2911-2917.

Rigolle, A., Van Den Abeele, K., & Foubert, I. (2018). Conventional and New Techniques to Monitor Lipid Crystallization. In K. Sato (Éd.), *Crystallization of Lipids* (p. 465-492). John Wiley & Sons, Ltd. https://doi.org/10.1002/9781118593882.ch17

Sängerlaub, S., Seibel, K., Miesbauer, O., Pant, A., Kiese, S., Rodler, N., Schmid, M., & Müller, K. (2018). Functional properties of foamed and/or stretched polypropylene-films containing sodium chloride particles for humidity regulation. *Polymer Testing*, *65*, 339-351. https://doi.org/10.1016/j.polymertesting.2017.12.002

Schertel, S., Salar-Behzadi, S., Karrer, J., Laggner, P., & Zimmer, A. (2021). Impact of polysorbate 65 on tripalmitin crystal growth and release stability of hot melt coated multiparticulate systems. *International Journal of Pharmaceutics*, 120970.

Siewert, M., Dressman, J., Brown, C. K., Shah, V. P., Aiache, J.-M., Aoyagi, N., Bashaw, D., Brown, C., Brown, W., & Burgess, D. (2003). FIP/AAPS guidelines to dissolution/in vitro release testing of novel/special dosage forms. *Aaps Pharmscitech*, *4*(1), 43-52.

Smith, P. R., Cebula, D. J., & Povey, M. J. (1994). The effect of lauric-based molecules on trilaurin crystallization. *Journal of the American Oil Chemists' Society*, *71*(12), 1367-1372.

Smith, P. R., & Povey, M. J. W. (1997). The effect of partial glycerides on trilaurin crystallization. *Journal of the American Oil Chemists' Society*, *74*(2), 169-171. https://doi.org/10.1007/s11746-997-0164-3

Takeguchi, S., Sato, A., Hondoh, H., Aoki, M., Uehara, H., & Ueno, S. (2020). Multiple β Forms of Saturated Monoacid Triacylglycerol Crystals. *Molecules*, *25*(21), 5086. https://doi.org/10.3390/molecules25215086

Vithani, K., Goyanes, A., Jannin, V., Basit, A. W., Gaisford, S., & Boyd, B. J. (2019). A proof of concept for 3D printing of solid lipid-based formulations of poorly water-soluble drugs to control formulation dispersion kinetics. *Pharmaceutical research*, *36*(7), 1-13.

Watanabe, Y., Zhao, W., Matsumoto, Y., Suda, M., Takayama, K., Ohgawara, Y., Kobayashi, Y., & Matsumoto, M. (1993). Increasing bioavailability of nifedipine from matrix granules prepared using macrogol and trilaurin. *International journal of pharmaceutics*, *99*(2-3), 337-341.

Windbergs, M., Strachan, C. J., & Kleinebudde, P. (2009a). Influence of structural variations on drug release from lipid/polyethylene glycol matrices. *European Journal of Pharmaceutical Sciences*, *37*(5), 555-562. https://doi.org/10.1016/j.ejps.2009.04.010

Windbergs, M., Strachan, C. J., & Kleinebudde, P. (2009b). Investigating the principles of recrystallization from glyceride melts. *Aaps Pharmscitech*, *10*(4), 1224-1233.

Windbergs, M., Strachan, C. J., & Kleinebudde, P. (2009c). Tailor-made dissolution profiles by extruded matrices based on lipid polyethylene glycol mixtures. *Journal of Controlled Release*, *137*(3), 211-216.

Windbergs, M., Strachan, C. J., & Kleinebudde, P. (2009d). Understanding the solid-state behaviour of triglyceride solid lipid extrudates and its influence on dissolution. *European Journal of Pharmaceutics and Biopharmaceutics*, *71*(1), 80-87.

Witzleb, R., Müllertz, A., Kanikanti, V.-R., Hamann, H.-J., & Kleinebudde, P. (2012). Dissolution of solid lipid extrudates in biorelevant media. *International journal of pharmaceutics*, *422*(1-2), 116-124.

Yoshikawa, S. (2016). *Effects of adding foreign particles on crystallization and physical properties of fat-based products*. https://doi.org/10.14989/doctor.r13044

Yoshikawa, S., Kida, H., & Sato, K. (2014). Promotional Effects of New Types of Additives on Fat Crystallization. *Journal of Oleo Science*, *63*(4), 333-345. https://doi.org/10.5650/jos.ess13155

Yoshikawa, S., Kida, H., & Sato, K. (2015). Fat crystallization with talc particles is influenced by particle size, concentration, and cooling rate. *European Journal of Lipid Science and Technology*, *117*(6), 858-868. https://doi.org/10.1002/ejlt.201400420

Yoshitomi, H., Nishihata, T., Frederick, G., Dillsaver, M., & Higuchi, L. T. (2011). Effect of triglyceride on small intestinal absorption of cefoxitin in rats. *Journal of Pharmacy and Pharmacology*, *39*(11), 887-891. https://doi.org/10.1111/j.2042-7158.1987.tb03123.x

Yoshitomi, H., Shizuku, Y., Masuda, Y., Itakura, R., Kanke, M., Okamoto, S., Nishihata, T., & Goto, S. (1992). Evaluation of Enteric Coated Tablet Sensitive to Pancreatic Lipase. I, In Vitro Disintegration Test. *Chemical and Pharmaceutical Bulletin*, *40*(7), 1902-1905. https://doi.org/10.1248/cpb.40.1902

Yoshitomi, H., Shizuku, Y., Masuda, Y., Itakura, R., Okamoto, S., Tomida, H., Nishihata, T., & Goto, S. (1993). Evaluation of Enteric Coated Tablet Sensitive to Pancreatic Lipase. II. In vivo Evaluation. *Biological and Pharmaceutical Bulletin*, *16*(12), 1260-1263. https://doi.org/10.1248/bpb.16.1260

Yuksel, N. (2000). Comparison of in vitro dissolution profiles by ANOVA-based, model-dependent and -independent methods. *International Journal of Pharmaceutics*, *209*(1-2), 57-67. https://doi.org/10.1016/S0378-5173(00)00554-8

Supplementary information

2.3.2.1. Measurements of solidification time lag and film formation

	0 s	*30 s*	*60 s*	*150 s*	*300 s*	*450 s*
III-1F / NaCl				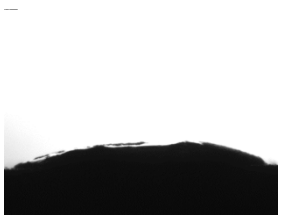		
	0 s	*30 s*	*60 s*	*150 s*	*300 s*	*450 s*
III-1F / III-1F	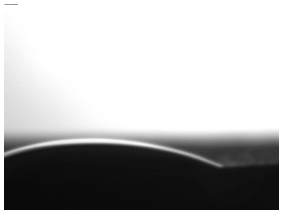	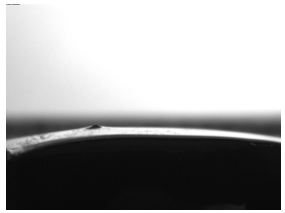	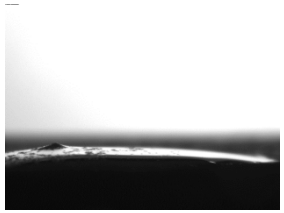	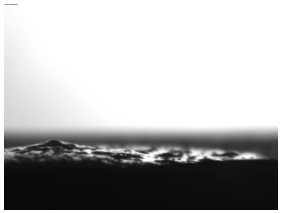		
	3 s	*30 s*	*60 s*	*150 s*	*300 s*	*450 s*
III-2F / NaCl		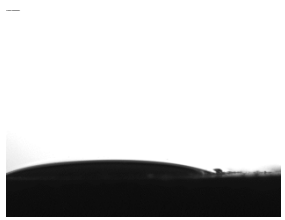	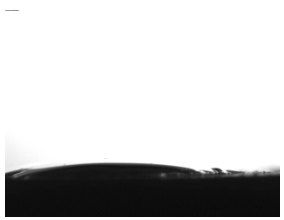			

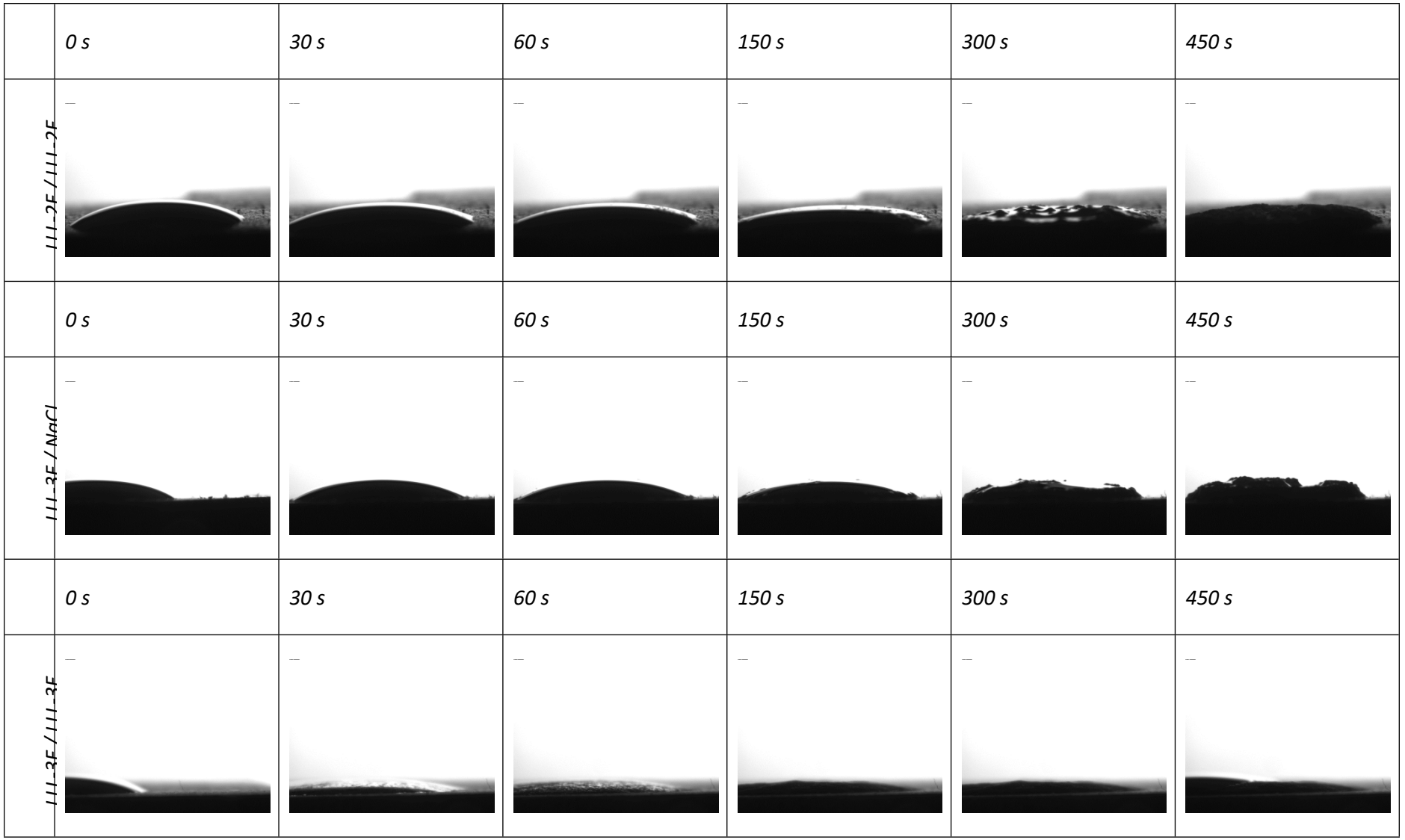

Figure S1. Observations of solidification & film formation of a molten droplet of formulation deposited on surface of NaCl or formulation itself at 30°C